4. RESULT AND DISCUSSION

4.1 Cyclic voltammetry

Stannous ions, Sn(II) was introduced into the BMPOTF ionic liquid along with $(CH_3SO_3)_2Sn$. The tin concentration was varied from 0.1 M to 0.5 M with 0.1 M interval. Cyclic voltammetry was swept from 0 to -1.0 V vs. Ag|AgCl then the sweep direction was reversed. The potential sweep rate was remained at 50 mVs^{-1} throughout the experiments. The diffusion coefficient of stannous ions in BMPOTF ionic liquid was calculated from the Randles-Sevcik equation.

$$I_p = (2.69 \times 10^5)\, n^{3/2} A D^{1/2} C\upsilon^{1/2} \qquad \textbf{(4.1)}$$

where;

I_p = peak current density (A/cm^2)

n = number of electron

A = electrode area (cm^2), 0.1257 cm^2

C = concentration ($mol\ cm^{-3}$)

D = diffusion coefficient ($cm^2\ s^{-1}$)

υ = scan rate ($V\ s^{-1}$)

Figure 4.1-4.5 show the voltametric response for BMPOTF with different tin concentration. Cyclic voltammetry was swept from 0 to -1.0 V vs. Ag|AgCl then the sweep direction was reversed. The potential sweep rate was remained at 50 mVs^{-1} throughout the experiments. Increasing stannous concentration produces a stronger reduction and oxidation peak. A single reduction and oxidation peak were observed in the cyclic voltammetry of tin deposition and dissolution at a copper substrate.

The forward sweep from 0 to -1 V vs. Ag-AgCl shows a reduction peak for tin deposition corresponding to a two-electron step:

Cathodic: $Sn^{2+} + 2e^- \rightarrow Sn$ **(4.2)**

On reversing the potential sweep from -1.0 V to 0 V vs. Ag-AgCl, a single stripping peak was observed confirming the two-electron oxidation of metallic to stannous ions via the reverse reaction:

Anodic: $Sn \rightarrow Sn^{2+} + 2e^-$ **(4.3)**

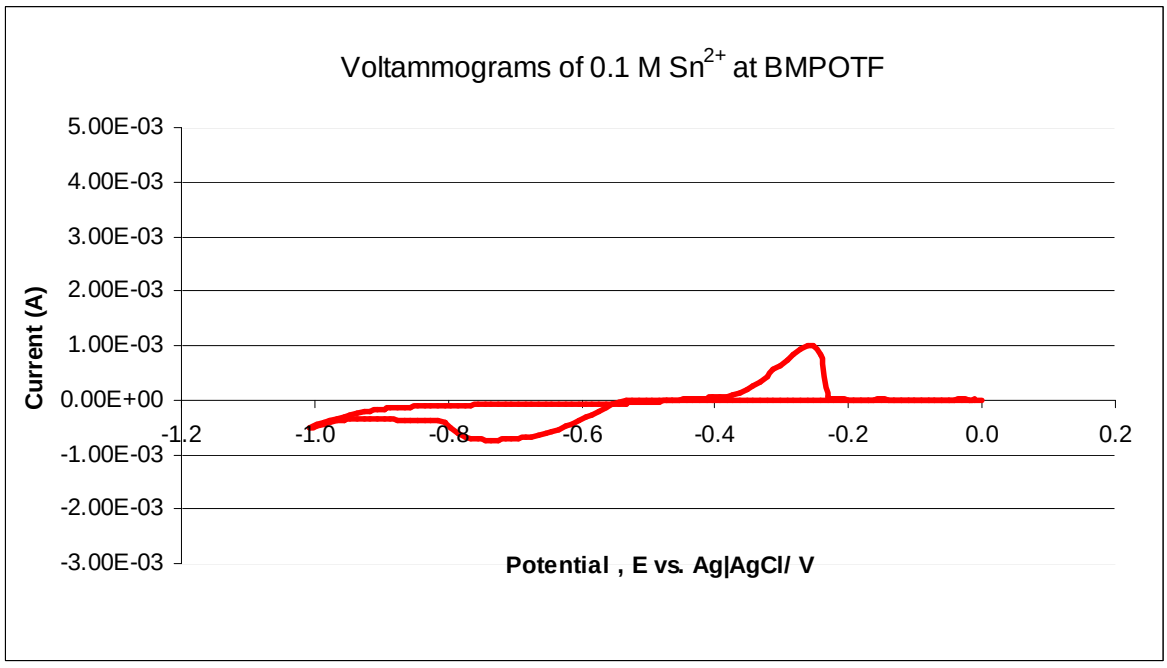

Figure 4.1: Voltammograms of 0.1 M Sn^{2+} at BMPOTF, potential sweep rate at 50 mVs^{-1}

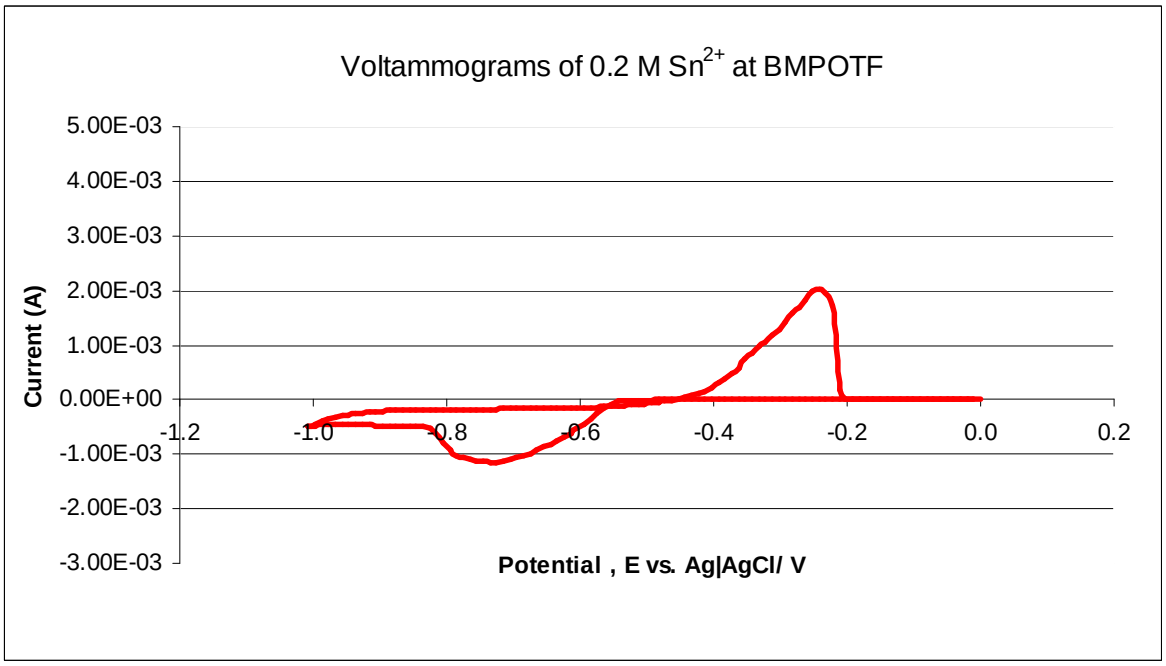

Figure 4.2: Voltammograms of 0.2 M Sn^{2+} at BMPOTF, potential sweep rate at 50 mVs^{-1}

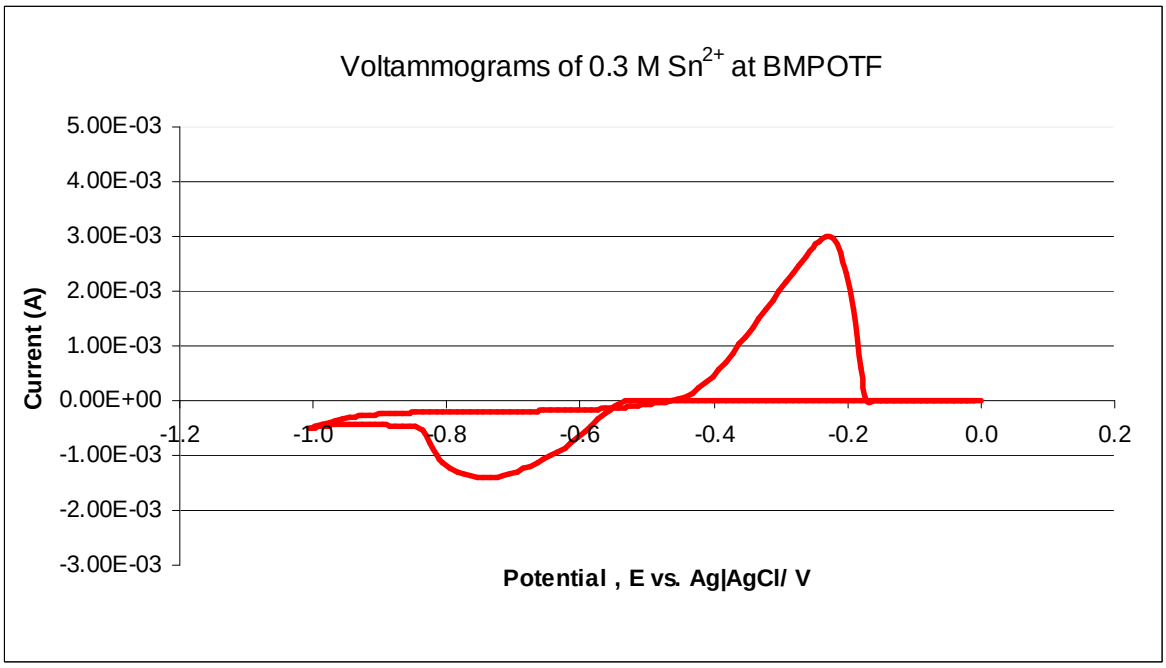

Figure 4.3: Voltammograms of 0.3 M Sn^{2+} at BMPOTF, potential sweep rate at 50 mVs^{-1}

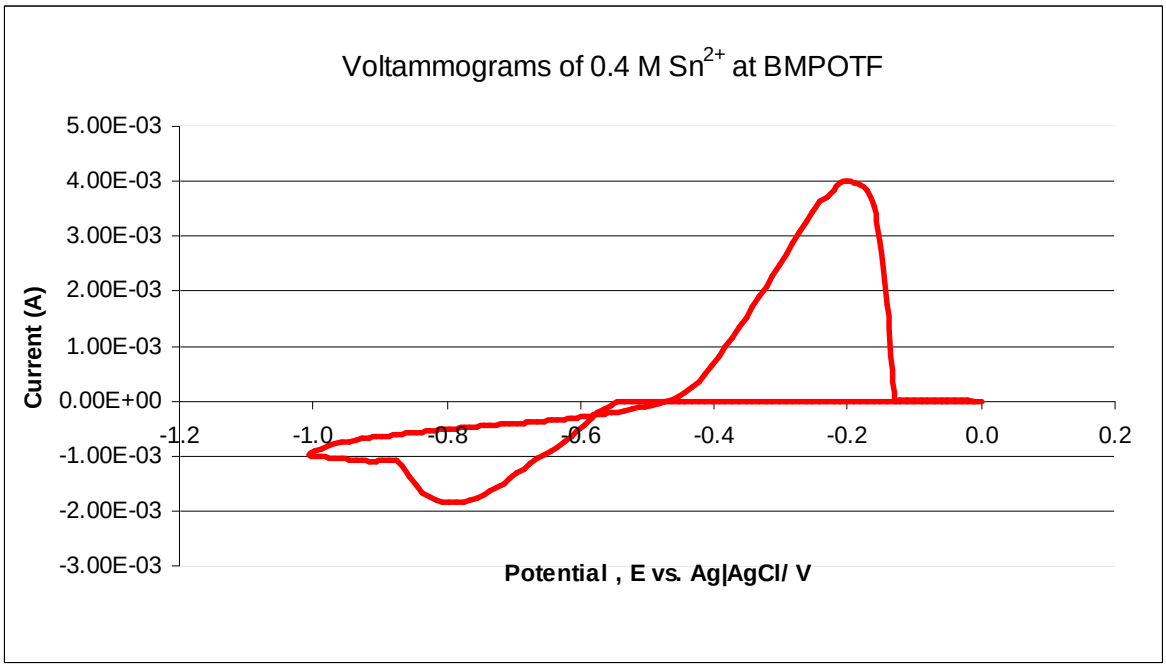

Figure 4.4: Voltammograms of 0.4 M Sn^{2+} at BMPOTF, potential sweep rate at 50 mVs^{-1}

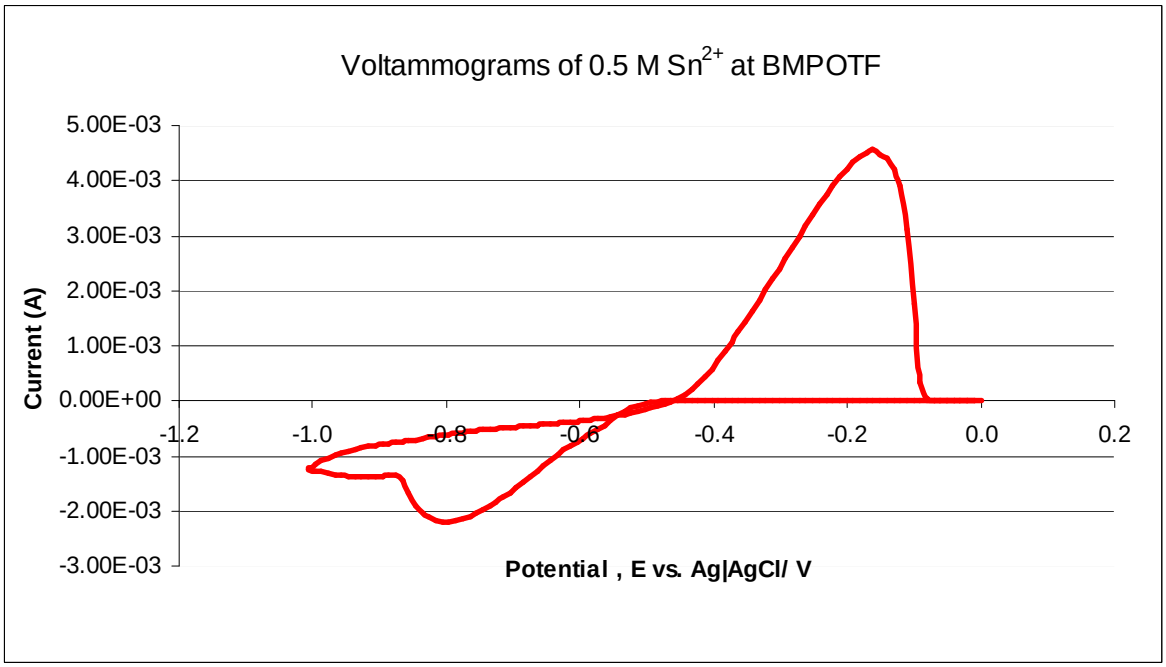

Figure 4.5: Voltammograms of 0.5 M Sn^{2+} at BMPOTF, potential sweep rate at 50 mVs^{-1}

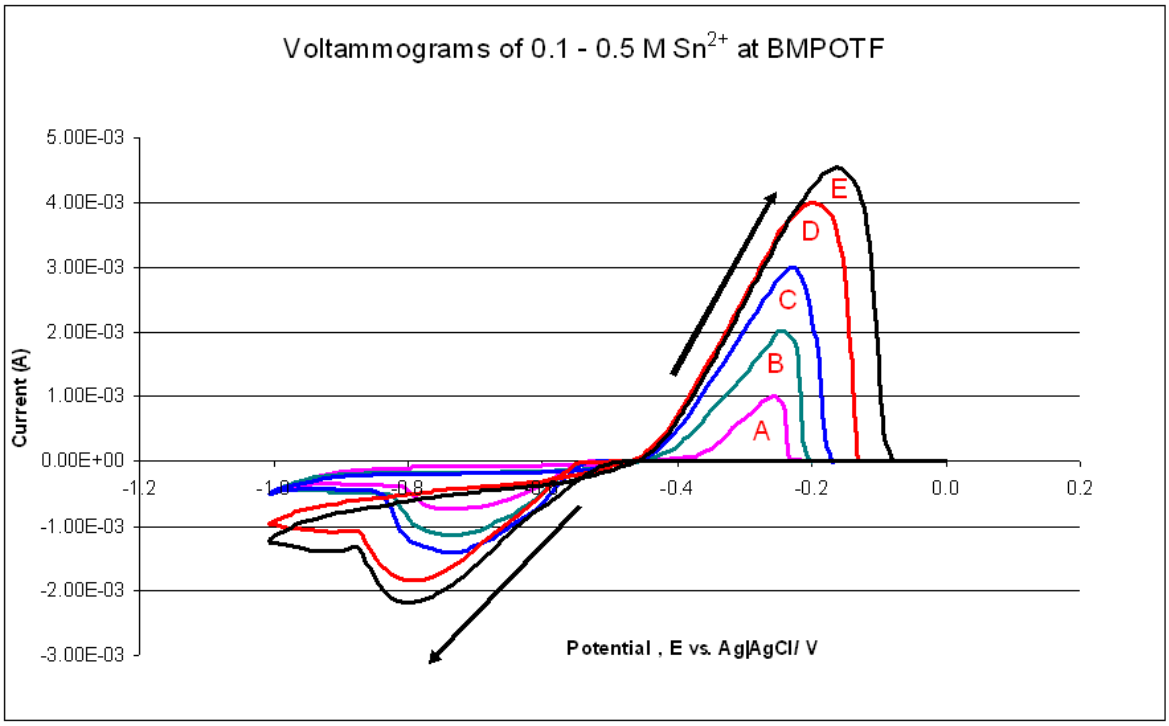

Figure 4.6: Cyclic voltammogram at 50 mVs^{-1} for solution ***X*** M $(CH_3SO_3)_2Sn$, A=0.1M, B=0.2M, C=0.3M, D=0.4M, E=0.5M

Concentration (mol/dm^3)	Peak Current (A)	Electrode area (cm^2)	Current Density (mA/cm^2)	Potential sweep rate, (mVs^{-1})	Diffusion of coefficient, (cm^2/s)
0.1	0.0009890	0.1257	7.86919	50	2.1394E-07
0.2	0.0020180	0.1257	16.05665	50	2.2268E-07
0.3	0.0029910	0.1257	23.79854	50	2.1742E-07
0.4	0.0039980	0.1257	31.81095	50	2.1851E-07
0.5	0.0045680	0.1257	36.34628	50	1.8256E-07
			Average		**2.11E-07**

Table 4.1: Peak current density and tin diffusion coefficient obtained at different Sn^{2+} concentration

The diffusion coefficient of stannous ions in BMPOTF ionic liquid is approximately

2.11×10^{-7} cm^2/s and was calculated from the Randles-Sevcik equation:

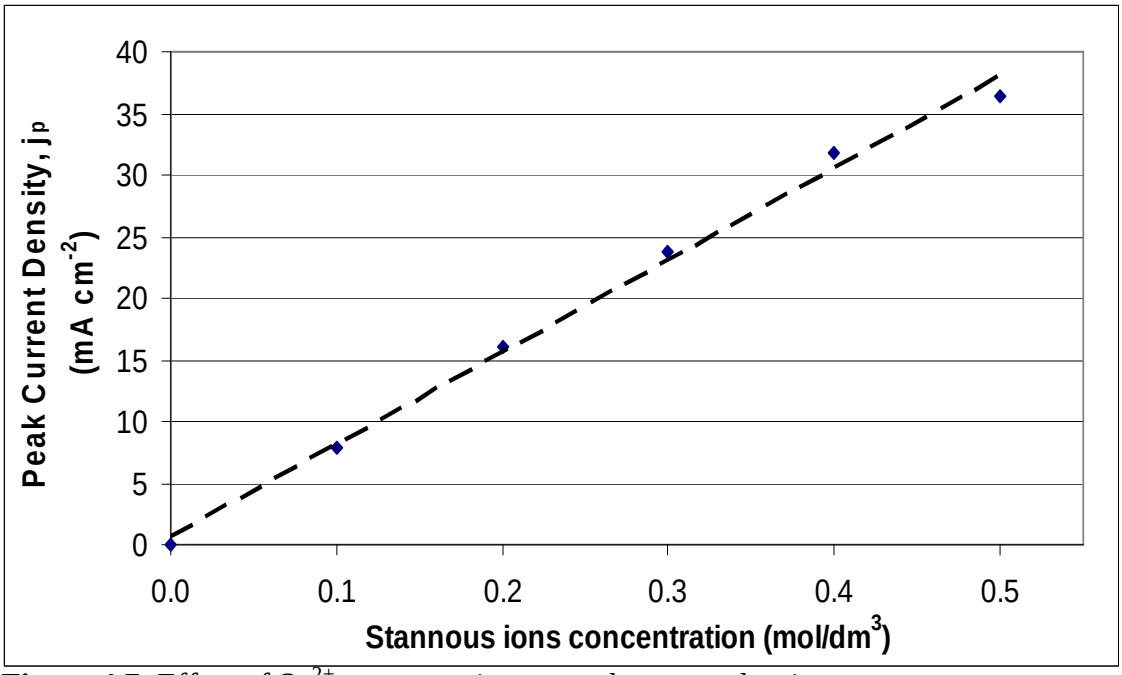

Figure 4.7: Effect of Sn^{2+} concentration on peak current density

Based on data in **Table 4.1**, tin diffusion coefficient, *D* has dropped when the mixture of BMPOTF and MSA tin had reached 0.5 M Sn^{2+}. From **Figure 4.7**, I_p increases with directly proportional to stannous concentration. The relationship to concentration is particularly important in analytical application and in studies of electrode mechanisms.

4.2 Chronoamperometry

As is known, the extent of diffusion layer thickness is time dependent [30]. Thus, the diffusion coefficient, D was counter evaluated by performing chronoamperometry experiments. **Figure 4.8-4.17** show an i-t transient during the reduction of Tin ions (Sn^{2+}) on working electrode at potential -0.8 V vs. SCE. By selecting the data points from the experimental data detected in **Table 4.2-4.6**, a Cottrell plot is obtained as current vs. minus square root of time.

The diffusion of coefficient was computed with the Cottrell equation as below:

$$i(t) = \frac{nFAD^{1/2}C}{\pi^{1/2}t^{1/2}} \qquad \textbf{(4.4)}$$

Where

i = current, in unit A

n = number of electrons (to reduce/oxidize one molecule of analyte j, for example)

F = Faraday constant, 96,485 C/mol

A = area of the (planar) electrode in cm^2, 0.1257 cm^2

C = initial concentration of the reducible analyte j in mol/cm^3;

D = diffusion coefficient in cm^2/s

t = time in s

Time (s)	$t^{-1/2}$ ($s^{-1/2}$)	Current (A)	Electrode area (cm^2)	Current Density (A/cm^2)	Diffusion of coefficient, (cm^2/s)
0	-	2.832E-04	0.1257	0.00225	-
1	1.0000	9.480E-05	0.1257	0.00075	3.0393E-07
2	0.7071	6.145E-05	0.1257	0.00049	2.5541E-07
3	0.5774	4.904E-05	0.1257	0.00039	2.4400E-07
4	0.5000	4.068E-05	0.1257	0.00032	2.2386E-07
5	0.4472	3.603E-05	0.1257	0.00029	2.1951E-07
6	0.4082	3.273E-05	0.1257	0.00026	2.1737E-07
7	0.3780	3.024E-05	0.1257	0.00024	2.1648E-07
8	0.3536	2.813E-05	0.1257	0.00022	2.1409E-07
9	0.3333	2.641E-05	0.1257	0.00021	2.1230E-07
10	0.3162	2.497E-05	0.1257	0.00020	2.1086E-07
11	0.3015	2.372E-05	0.1257	0.00019	2.0931E-07
12	0.2887	2.266E-05	0.1257	0.00018	2.0838E-07
13	0.2774	2.169E-05	0.1257	0.00017	2.0684E-07
14	0.2673	2.085E-05	0.1257	0.00017	2.0583E-07
15	0.2582	2.011E-05	0.1257	0.00016	2.0515E-07
				Average	**2.2355E-07**

Table 4.2: Chronoamperometry data of 0.1 M Sn^{2+} at BMPOTF

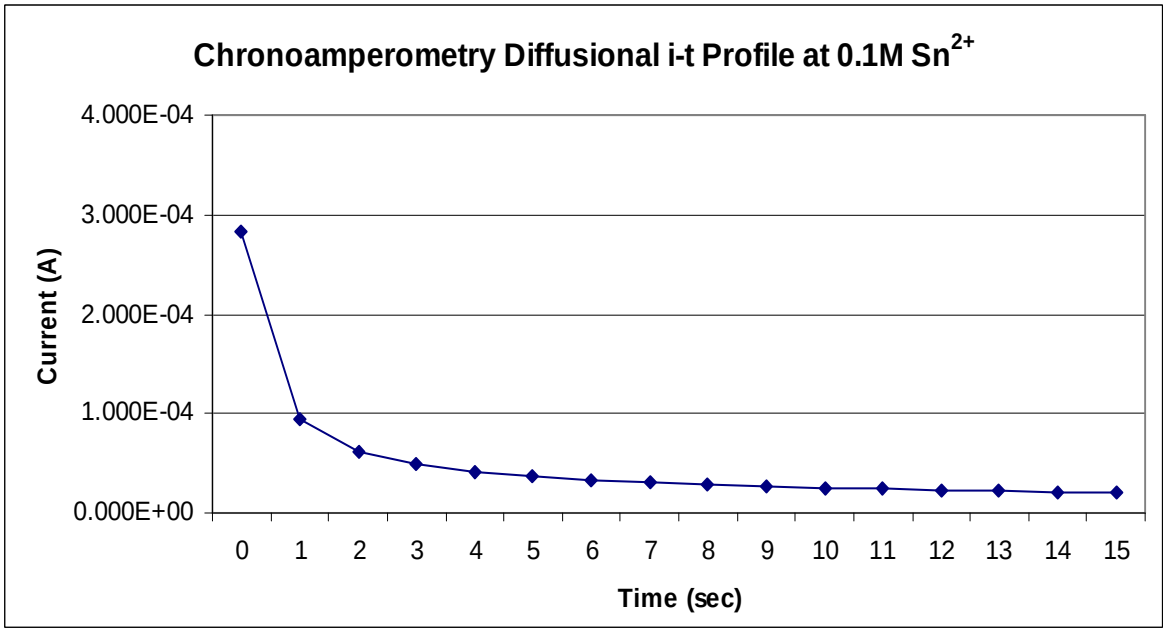

Figure 4.8: Chronoamperometry profile i vs. t, 0.1 M Sn^{2+} at BMPOTF

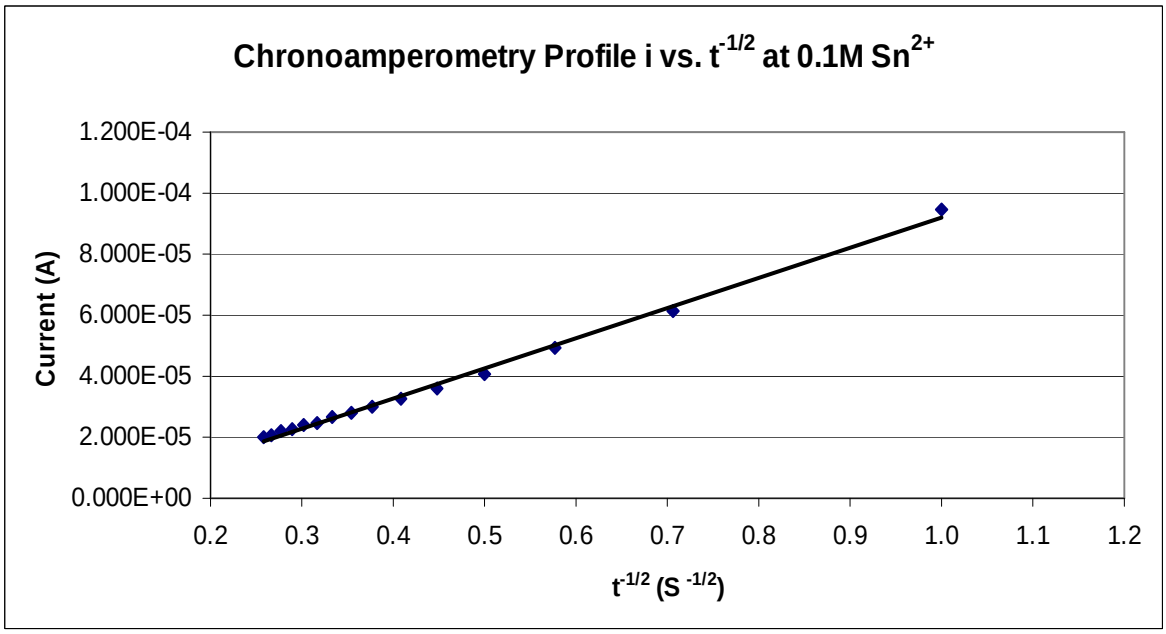

Figure 4.9: Chronoamperometry profile i vs. $t^{-1/2}$, 0.1 M Sn^{2+} at BMPOTF

Time (s)	$t^{-1/2}$ ($s^{-1/2}$)	Current (A)	Electrode area (cm^2)	Current Density (A/cm^2)	Diffusion of coefficient, (cm^2/s)
0	-	4.833E-04	0.1257	0.00385	-
1	1.0000	2.010E-04	0.1257	0.00160	3.4158E-07
2	0.7071	1.253E-04	0.1257	0.00100	2.6548E-07
3	0.5774	1.003E-04	0.1257	0.00080	2.5517E-07
4	0.5000	8.665E-05	0.1257	0.00069	2.5392E-07
5	0.4472	7.720E-05	0.1257	0.00061	2.5195E-07
6	0.4082	6.996E-05	0.1257	0.00056	2.4829E-07
7	0.3780	6.454E-05	0.1257	0.00051	2.4652E-07
8	0.3536	6.079E-05	0.1257	0.00048	2.4995E-07
9	0.3333	5.633E-05	0.1257	0.00045	2.4145E-07
10	0.3162	5.338E-05	0.1257	0.00042	2.4091E-07
11	0.3015	5.061E-05	0.1257	0.00040	2.3821E-07
12	0.2887	4.833E-05	0.1257	0.00038	2.3698E-07
13	0.2774	4.684E-05	0.1257	0.00037	2.4115E-07
14	0.2673	4.534E-05	0.1257	0.00036	2.4333E-07
15	0.2582	4.383E-05	0.1257	0.00035	2.4363E-07
				Average	***2.5323E-07***

Table 4.3: Chronoamperometry data of 0.2 M Sn^{2+} at BMPOTF

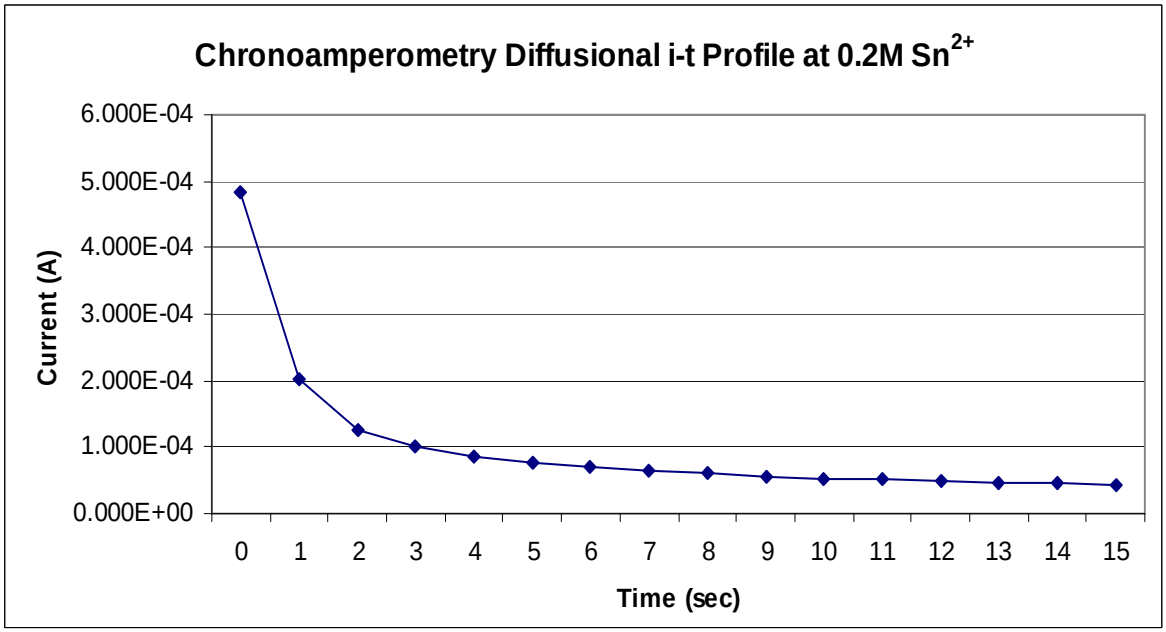

Figure 4.10: Chronoamperometry profile i vs. t, 0.2 M Sn^{2+} at BMPOTF

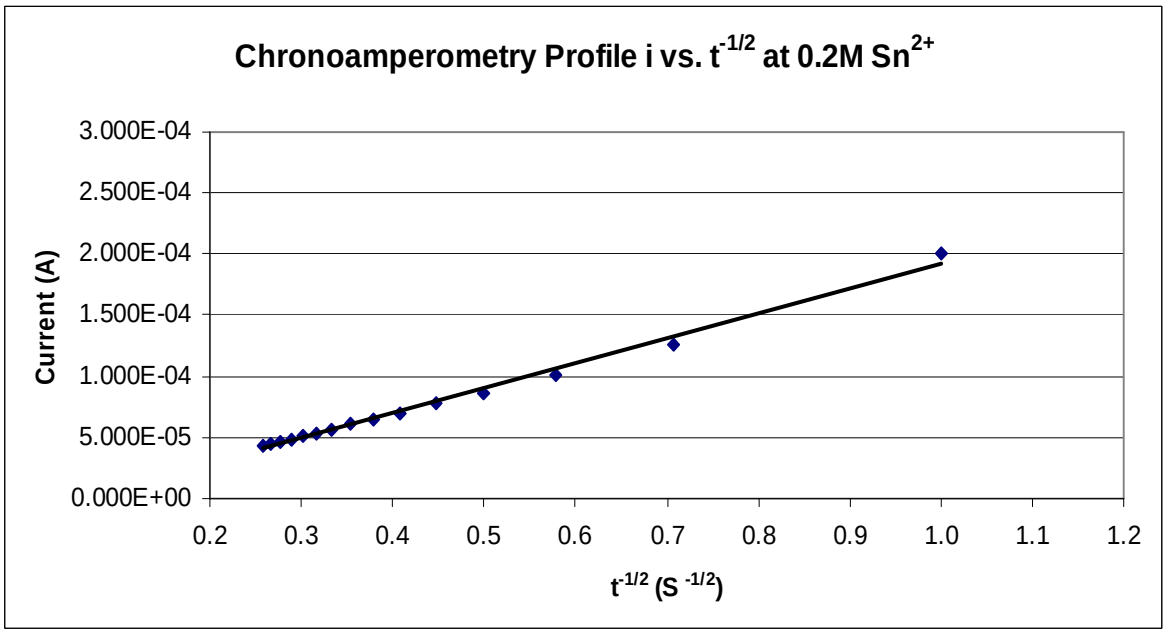

Figure 4.11: Chronoamperometry profile i vs. $t^{-1/2}$, 0.2 M Sn^{2+} at BMPOTF

Time (s)	$t^{-1/2}$ ($s^{-1/2}$)	Current (A)	Electrode area (cm^2)	Current Density (A/cm^2)	Diffusion of coefficient, (cm^2/s)
0	-	7.466E-04	0.1257	0.00594	-
1	1.0000	3.329E-04	0.1257	0.00265	4.1643E-07
2	0.7071	2.110E-04	0.1257	0.00168	3.3459E-07
3	0.5774	1.662E-04	0.1257	0.00132	3.1139E-07
4	0.5000	1.394E-04	0.1257	0.00111	2.9208E-07
5	0.4472	1.211E-04	0.1257	0.00096	2.7554E-07
6	0.4082	1.095E-04	0.1257	0.00087	2.7033E-07
7	0.3780	1.006E-04	0.1257	0.00080	2.6620E-07
8	0.3536	9.394E-05	0.1257	0.00075	2.6528E-07
9	0.3333	8.669E-05	0.1257	0.00069	2.5416E-07
10	0.3162	8.207E-05	0.1257	0.00065	2.5310E-07
11	0.3015	7.810E-05	0.1257	0.00062	2.5212E-07
12	0.2887	7.570E-05	0.1257	0.00060	2.5840E-07
13	0.2774	7.258E-05	0.1257	0.00058	2.5733E-07
14	0.2673	6.986E-05	0.1257	0.00056	2.5675E-07
15	0.2582	6.634E-05	0.1257	0.00053	2.4806E-07
				Average	***2.8078E-07***

Table 4.4: Chronoamperometry data of 0.3 M Sn^{2+} at BMPOTF

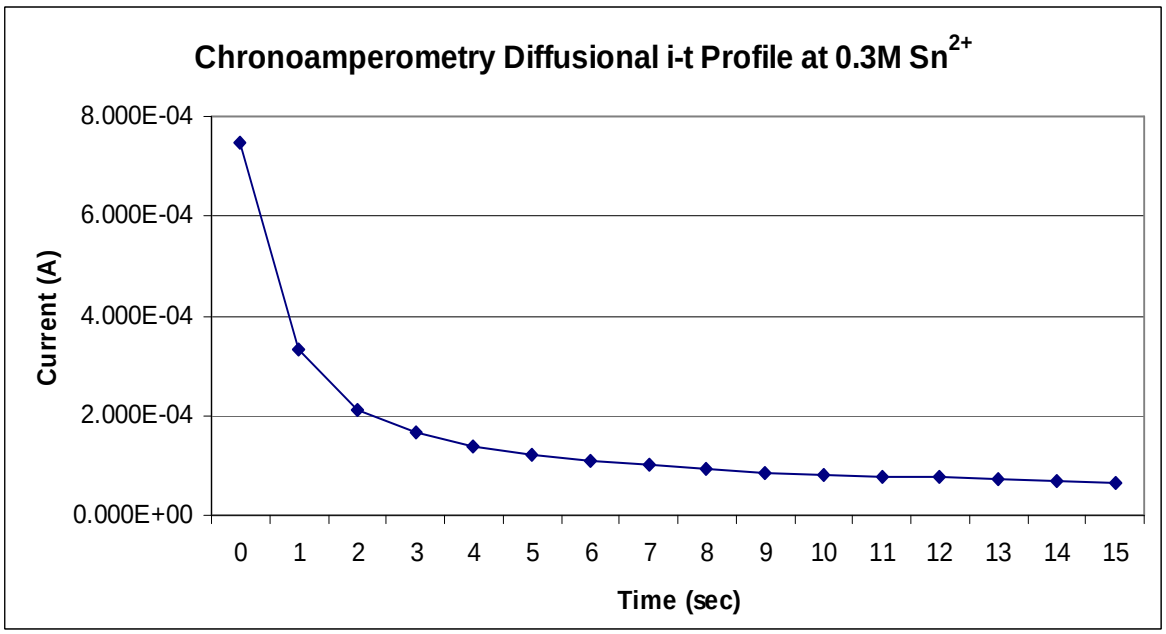

Figure 4.12: Chronoamperometry profile i vs. t, 0.3 M Sn^{2+} at BMPOTF

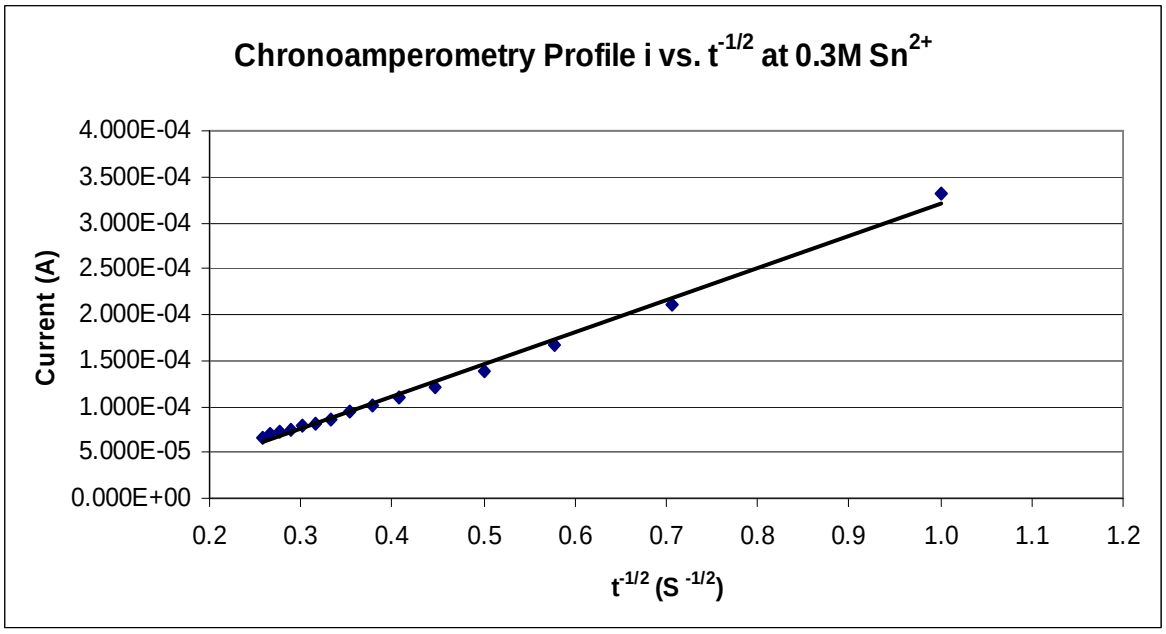

Figure 4.13: Chronoamperometry profile i vs. $t^{-1/2}$, 0.3 M Sn^{2+} at BMPOTF

Time (s)	$t^{-1/2}$ ($s^{-1/2}$)	Current (A)	Electrode area (cm^2)	Current Density (A/cm^2)	Diffusion of coefficient, (cm^2/s)
0	-	9.165E-04	0.1257	0.00729	-
1	1.0000	4.473E-04	0.1257	0.00356	4.2290E-07
2	0.7071	2.882E-04	0.1257	0.00229	3.5112E-07
3	0.5774	2.306E-04	0.1257	0.00183	3.3720E-07
4	0.5000	1.958E-04	0.1257	0.00156	3.2414E-07
5	0.4472	1.691E-04	0.1257	0.00135	3.0220E-07
6	0.4082	1.514E-04	0.1257	0.00120	2.9070E-07
7	0.3780	1.384E-04	0.1257	0.00110	2.8341E-07
8	0.3536	1.276E-04	0.1257	0.00102	2.7532E-07
9	0.3333	1.176E-04	0.1257	0.00094	2.6309E-07
10	0.3162	1.116E-04	0.1257	0.00089	2.6325E-07
11	0.3015	1.061E-04	0.1257	0.00084	2.6174E-07
12	0.2887	1.016E-04	0.1257	0.00081	2.6182E-07
13	0.2774	9.768E-05	0.1257	0.00078	2.6218E-07
14	0.2673	9.409E-05	0.1257	0.00075	2.6197E-07
15	0.2582	9.109E-05	0.1257	0.00072	2.6307E-07
				Average	***2.9494E-07***

Table 4.5: Chronoamperometry data of 0.4 M Sn^{2+} at BMPOTF

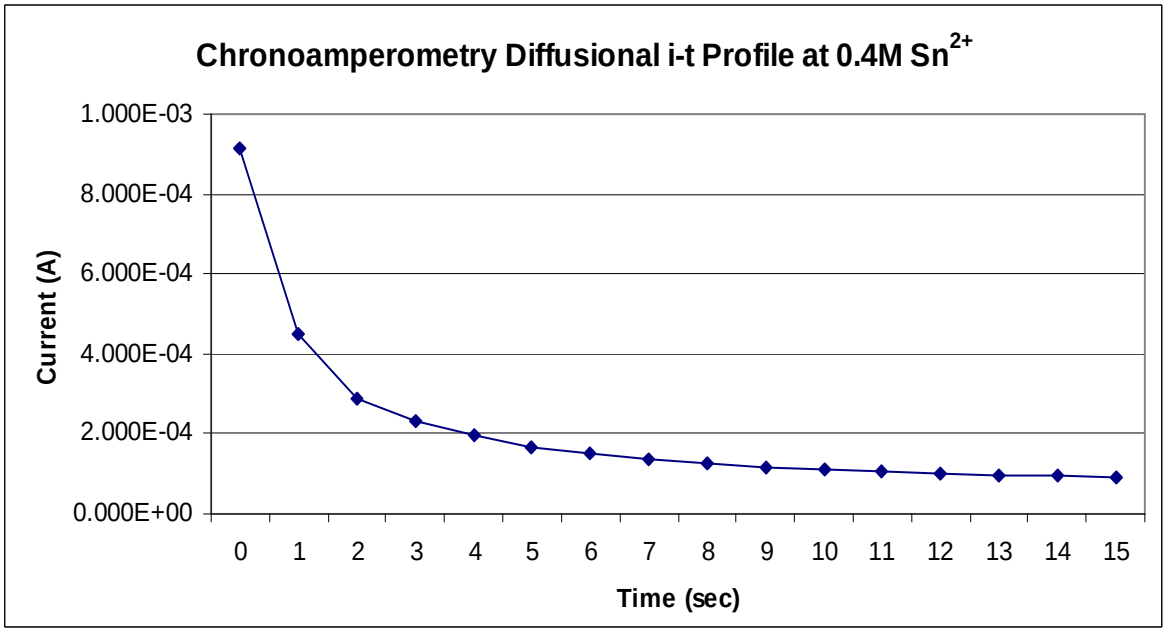

Figure 4.14: Chronoamperometry profile i vs. t, 0.4 M Sn^{2+} at BMPOTF

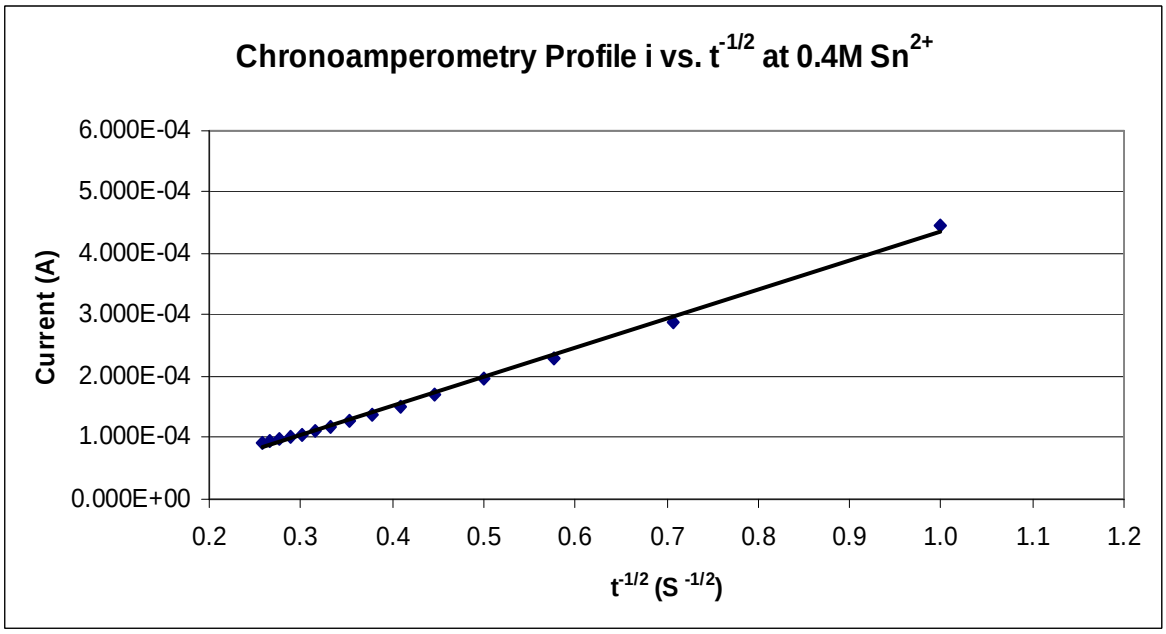

Figure 4.15: Chronoamperometry profile i vs. $t^{-1/2}$, 0.4 M Sn^{2+} at BMPOTF

Time (s)	$t^{-1/2}$ ($s^{-1/2}$)	Current (A)	Electrode area (cm^2)	Current Density (A/cm^2)	Diffusion of coefficient, (cm^2/s)
0	-	9.698E-04	0.1257	0.00772	-
1	1.0000	5.325E-04	0.1257	0.00424	3.8358E-07
2	0.7071	3.227E-04	0.1257	0.00257	2.8174E-07
3	0.5774	2.570E-04	0.1257	0.00204	2.6805E-07
4	0.5000	2.198E-04	0.1257	0.00175	2.6142E-07
5	0.4472	1.943E-04	0.1257	0.00155	2.5535E-07
6	0.4082	1.741E-04	0.1257	0.00139	2.4602E-07
7	0.3780	1.610E-04	0.1257	0.00128	2.4545E-07
8	0.3536	1.509E-04	0.1257	0.00120	2.4643E-07
9	0.3333	1.416E-04	0.1257	0.00113	2.4411E-07
10	0.3162	1.340E-04	0.1257	0.00107	2.4290E-07
11	0.3015	1.281E-04	0.1257	0.00102	2.4418E-07
12	0.2887	1.237E-04	0.1257	0.00098	2.4839E-07
13	0.2774	1.186E-04	0.1257	0.00094	2.4736E-07
14	0.2673	1.141E-04	0.1257	0.00091	2.4656E-07
15	0.2582	1.112E-04	0.1257	0.00088	2.5091E-07
				Average	***2.6083E-07***

Table 4.6: Chronoamperometry data of 0.5 M Sn^{2+} at BMPOTF

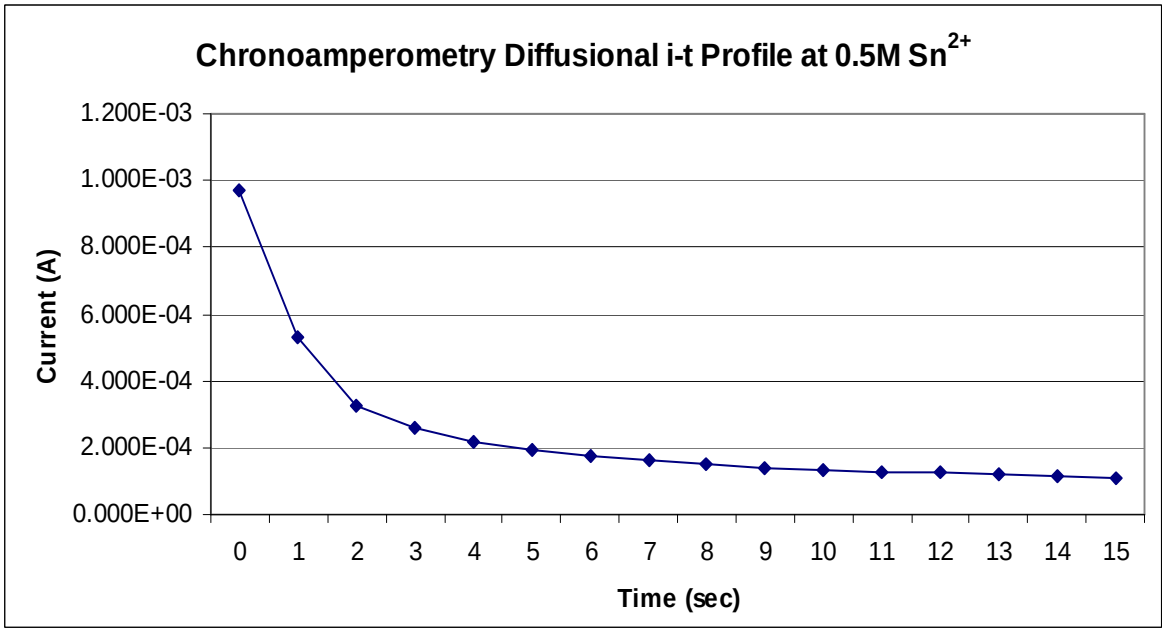

Figure 4.16: Chronoamperometry profile i vs. t, 0.5 M Sn^{2+} at BMPOTF

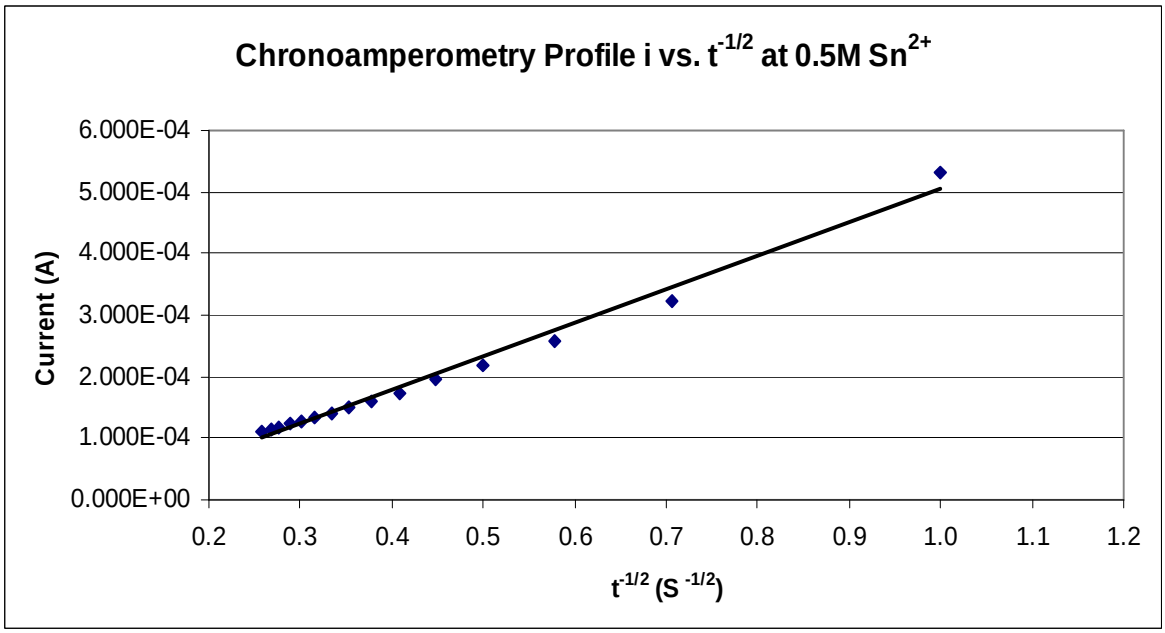

Figure 4.17: Chronoamperometry profile i vs. $t^{-1/2}$, 0.5 M Sn^{2+} at BMPOTF

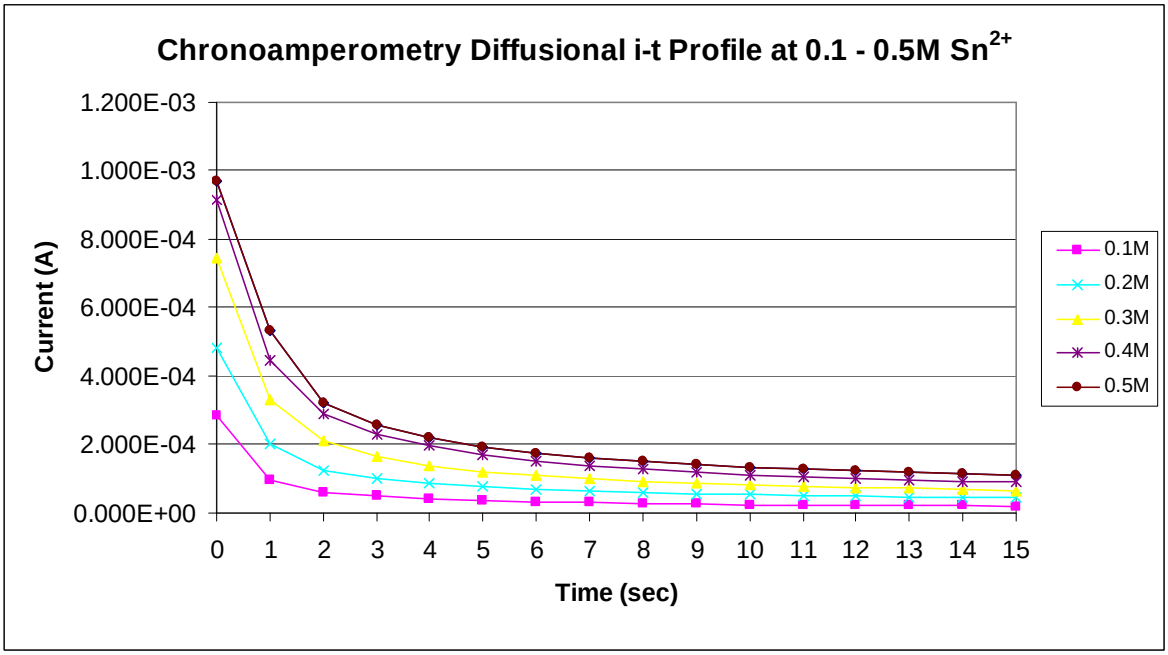

Figure 4.18: Chronoamperometry diffusional i-t profile from 0.1-0.5 M Sn^{2+} at BMPOTF

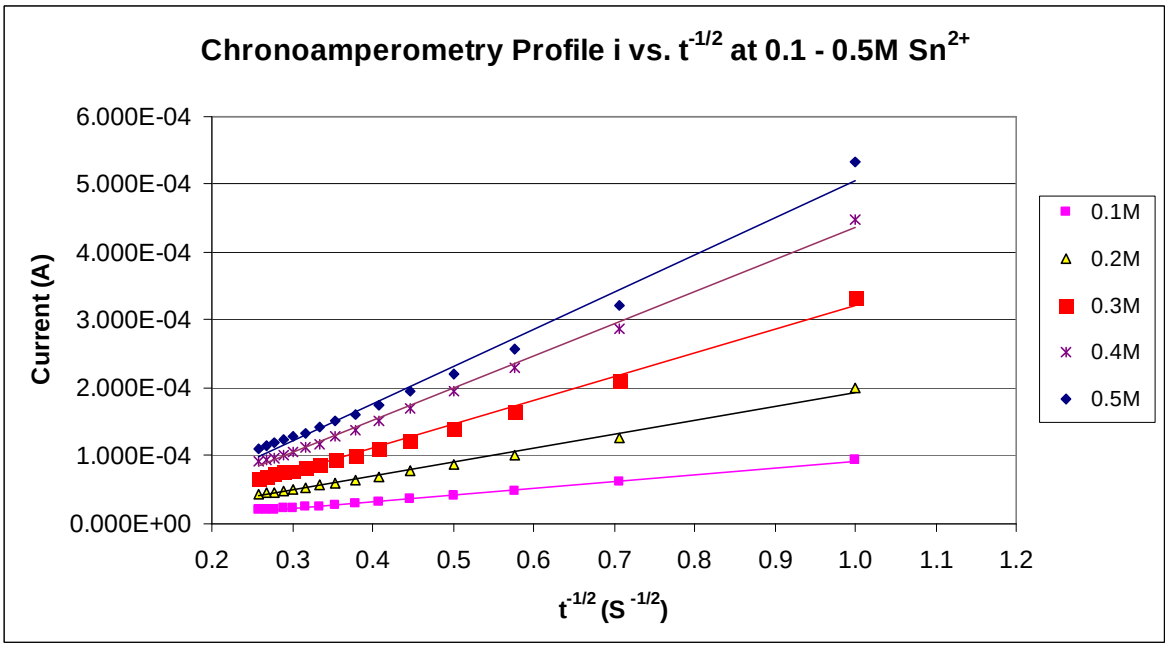

Figure 4.19: Chronoamperometry profile i vs. $t^{-1/2}$ from 0.1-0.5 M Sn^{2+} at BMPOTF

Sn^{2+} Molarity (mol/ dm^3)	Sn^{2+} Dif. coefficient, *D* (cm^2/s)
0.1	**2.2355E-07**
0.2	**2.5323E-07**
0.3	**2.8078E-07**
0.4	**2.9494E-07**
0.5	**2.6083E-07**
Average	**2.63×10^{-07}**

Table 4.7: Tin diffusion coefficient obtained at different Sn^{2+} concentration through Chronoamperometry- Cottrell equation

No.	Electrolyte	Anions	Reference	Sn^{2+} Dif. coefficient, *D* (cm^2/s)
1	Aqueos, CH_3SO_3H	$CH_3SO_3^-$	[3]	6.5×10^{-6}
2	1-ethyl-3-methylimidazolium tetrafluoroborate, $[EMIm]BF_4$	BF_4^-	[8]	6.1×10^{-7}
3	1-n-butyl-1-methylpyrrolidinium bis (trifluoromethylsulfonyl) imide, BMPTFSI	$TFSI^-$	[9]	1.0×10^{-7}
4	$AlCl_3$ with 1-methly-3-ethyl imidazolium chloride, $AlCl_3$-MeEtimCl	$SnCl_4^{2-}$	[7]	5.3×10^{-7}
5	1-butyl-1-methyl-pyrrolidinium trifluoro-methanesulfonate, BMPOTF	$CH_3SO_3^-$ and OTF^-	This work- Cyclic voltammetry	2.11×10^{-7}
			This work- Chronoamperometry	2.63×10^{-7}

Table 4.8: Tin diffusion coefficient based on literature review

The chronoamperograms revealed the presence of mixture of MSA tin and BMPOTF ionic liquid over the concentration range of 0.1-0.5 M. Plotting the net current vs. the minus square root of time gives a straight line. This indicates that a diffusion controlled process is dominant for tin as was demonstrated previously using cyclic voltammetry.

The values obtained from chronoamperometric experiment for the diffusion coefficient was having slight drop from 0.4 to 0.5 M of Sn^{2+}. This was in good agreement with the results obtained from cyclic voltammetry.

The dependency of the Diffusion coefficient to the viscosity and the radius of the diffusing species can be explained by the Stoke-Einstein equation, D= kT/ 6 ηr where k = Boltzmann constant, T = Kelvin temperature, η = viscosity of the solvent, r = dynamic radius of the diffusing species.

Hussey *et al.* [7] found that the Tin(II) exists as $SnCl_4^{2-}$ in $AlCl_3$ with 1-methly-3-ethyl imidazolium chloride ionic liquid and the low values of the diffusion coefficient was due to the increased viscosity of the ionic liquid. They also suggest that there is some degree of association between the Tin(II) with chloroaluminate ions such as $AlCl_4^-$ and $Al_2Cl_7^-$, which contribute to the low value of the diffusion coefficient.

W. Yang *et al.* [8] used tetrafluoroborate, BF_4^- based ionic liquid, where the diffusion coefficient was higher than calculated from the chloroaluminate ionic liquid by Hussey. From the Stoke-Einstein equation, it can be seen that the smaller Tin(II) tetrafluoroborate species will contribute to a slightly higher diffusion coefficient value for the Tin(II) species.

Studies using trifluoromethylsulfonyl imide ionic liquids from Tachikawa *et al.* [9] and this work using trifluoromethylsulfonate ionic liquid gave smaller diffusion coefficient for the Tin(II) species. It can be suggested that the complexation between the Tin(II) with trifluoromethylsulfonate and trifluoromethylsulfonyl imide, which is larger than the chloride ion and the tetrafluoroborate ion, has increased the radius of the Tin(II) species in solution. This contributes to the lower diffusion coefficient compared to the chloride and tetrafluoroborate based ionic liquids in the works previously reported [7,8].

4.3 Electroplating experiments

In electroplating industry, metals are electrodeposited using constant current (galvanostatic) methods. Constant current electrodeposition of tin on polished copper electrodes with area 8 cm^2 were carried out using current densities of 1, 2, 3, 4, 5, 6, and 7 A/ dm^2 (ASD). Stannous ions, Sn(II) was introduced into the BMPOTF ionic liquid along with $(CH_3SO_3)_2Sn$. The tin concentration was varied from 0.1 M to 0.5 M with 0.1 M interval.

The panels were weighted and attached to the circuit with a wire electrical contact. It was placed in the cell with a tin anode on both of its adjacent side. After electrodeposition, the panel was removed, rinsed in hot de-ionized water, dried and weighted. By using Faraday's law of electrolysis, the increase in mass of the copper panels after electrodeposition and the charge passed, the current efficiency can be estimated.

The current efficiency is defines as the proportion of the current that is used in a specified reaction: the unused part in this process is considered a waste. Thus, the current efficiency, ε is defined as the ratio of the specified chemical change to the total chemical change [9]. Thus,

$$\varepsilon\ (\%) = \frac{\text{Actual reaction}}{\text{Total reaction}} \text{ X } 100 \qquad \textbf{(4.5)}$$

The actual change is the mass of metal deposited or dissolved at the consumable anode, and theoretical change is the corresponding mass to be expected from Faraday's law of reaction if there were no side reaction. The efficiencies are not always 100% as hydrogen and oxygen are evolved at the cathode and the anode respectively.

Faraday's Law:

$$Q = I \cdot t \qquad \textbf{(4.6)}$$

$$m = \frac{Q}{qn} \cdot \frac{M}{N_A} = \frac{1}{qN_A} \cdot \frac{QM}{n}$$
$$= \frac{1}{F} \cdot \frac{QM}{n} = \frac{1}{96{,}485\, C \cdot mol^{-1}} \cdot \frac{QM}{n} \qquad \textbf{(4.7)}$$

Where,

m is the mass of the substance produced at the electrode (in grams);

Q is the total electric charge that passed through the solution (in coulombs);

q is the electron charge = 1.602×10^{-19} coulombs per electron;

n is the valence number of the substance as an ion in solution (electrons per ion),

F = qN$_A$ = 96,485 C· mol^{-1} is Faraday's constant,

M is the molar mass of the substance (in grams per mole), and

N$_A$ is Avogadro's number = 6.023×10^{23} ions per mole

Scanning electron microscopy (SEM), Energy dispersive X-ray spectroscopy (EDX) and Atomic Force Microscopy (AFM) were used to examine the surface morphology and analyze the elemental compositions of the electrodeposits.

No.	Current Density (A/dm^2)	Stannous Ions Concentration (mol/dm^3)				
		0.1	0.2	0.3	0.4	0.5
1	1.0	99.5	99.6	98.9	98.2	94.8
2	2.0	99.9	98.2	98.2	97.9	87.7
3	3.0	99.8	96.4	98.0	97.8	81.1
4	4.0	99.2	98.7	97.9	97.0	72.7
5	5.0	99.6	98.6	97.0	96.9	66.3
6	6.0	99.70	97.7	96.9	96.0	61.7
7	7.0	98.7	97.6	96.3	94.6	58.3

Table 4.9: Current efficiency obtained at different Sn^{2+} concentration

Theoretically, electrodeposition at higher current density (HCD) will decrease the current efficiency due to hydrogen evolution. However, tin electro deposition via the mixture of ionic liquid BMPOTF and Methane Sulfonic Acid (MSA) based tin methane sulfonate salts has shown excellent current efficiency which is as high as 99.9%.

Based on result in **Table 4.9**, the average current efficiency was $97 \pm 2\%$ when electrodeposited with Sn^{2+} concentration in the range of 0.1 - 0.4 M, and at 1 to 7 ASD. The deposit was dense, fine and in polygonal grain structure as revealed in **Figure 4.20, 4.23, 4.26 and 4.29**, SEM images @ 3500X. The grain size of tin had increased from 1-2 µm to$\approx$ 5 µm proportional to current density change. There was no copper element observed from the tin plated surface via EDX analysis at 20 keV. It had proven that the tin deposit on copper substrate is dense and compact.

However, there was a sudden drop for current efficiency when deposited with 0.5 M MSA tin. The similar phenomenon happened in cyclic voltammetry and chronoamperometry experiments whereby the stannous diffusion coefficient dropped when the mixture of BMPOTF and MSA tin had reached 0.5 M Sn^{2+}. It was believed

that the mixture of BMPOTF and MSA tin has reached saturated point at 0.5M Sn^{2+}. The ion H^+ from acid was reduced to hydrogen gas during tin deposition. The hydrogen gas was co-deposited onto the copper substrate, thus causing the tin deposit was dull, porous and had poor reflectivity as shown in **Figure 4.32**. The copper element was revealed at the tin plated surface when analyzed under 20 keV EDX as shown in **Figure 4.33 and 4.34**.

The SEM results that obtained in this work is similar to the study which carried out by Q. B. Zhang *et al.* [18]. Q. B. Zhang *et al.* have done the copper electrodeposition in an electrolyte which contains mixture of ionic liquid 1-butyl-3-methylimidazolium hydrogen sulfate-[BMIM]HSO_4, sulfuric acid, hydrated copper sulfate and distilled water. The surface morphology of the copper deposition in Q. B. Zhang *et al.* study showing that the grain is finer and dense with the increasing of ionic liquid ratio in electrolyte. It was believed that the ionic liquid is an efficient leveling agent in copper electrodeposition, leading to more leveled and fine grained cathodic deposits. The ionic liquid also inhibits crystal growth and promotes nucleation of copper, leading to finer grained copper deposits [18].

Representative AFM images of the tin deposition are seen in **Figure 4.35-4.39**. The copper samples were plated at different Sn^{2+} concentration in BMPOTF ionic liquid at 1 ASD. These images parallel the SEM images in **Figure 4.20, 4.23, 4.26, 4.29 and 4.32** but AFM images give a perspective of the third (***Z***) dimension. The roughness is increasing proportional to Sn^{2+} concentration. The smooth and fine structure can be observed from **Figure 4.35 and 4.36**. The roughness of deposit become slightly greater when plated at 0.3 and 0.4 M Sn^{2+} **(Figure 4.37 and 4.38)**. The larger tin crystal and deep crevice found at the sample plated at 0.5 M Sn^{2+} **(Figure 4.39)**.

The AFM surface morphology analysis in this work is identical with the study that carried out by M. J. Deng *et al.* [4]. M. J. Deng *et al.* has done the investigation on electrodeposition behavior of nickel. It was reported that the roughness of the nickel-deposited surface increased as the deposition potential and current density increased [4].

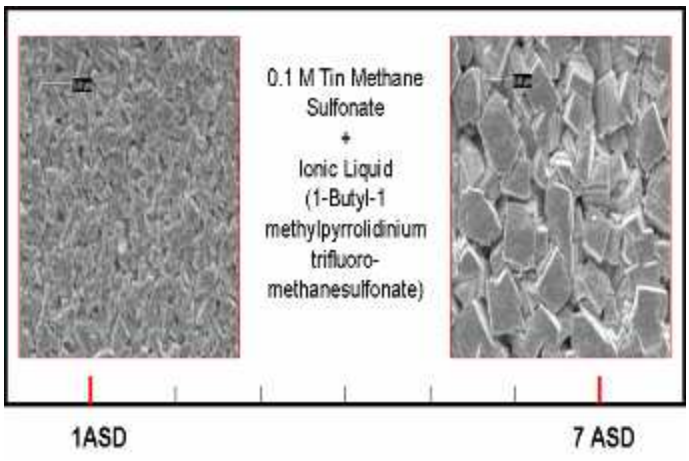

Figure 4.20: SEM for 0.1 M Sn^{2+} at BMPOTF with 1 ASD and 7 ASD electrodeposition

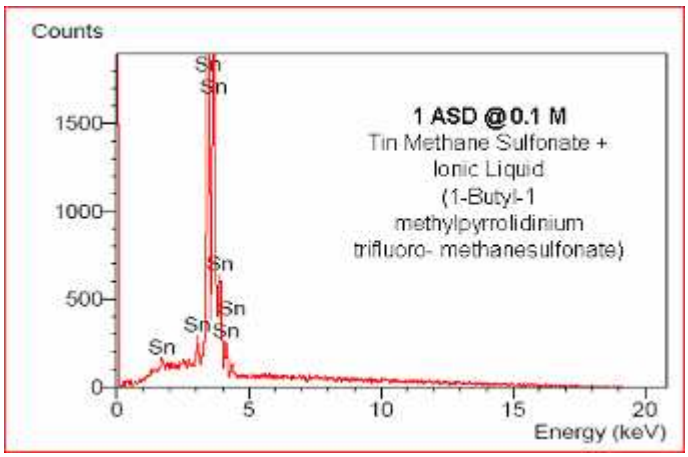

Figure 4.21: EDX for 0.1 M Sn^{2+} at BMPOTF with 1 ASD electrodeposition

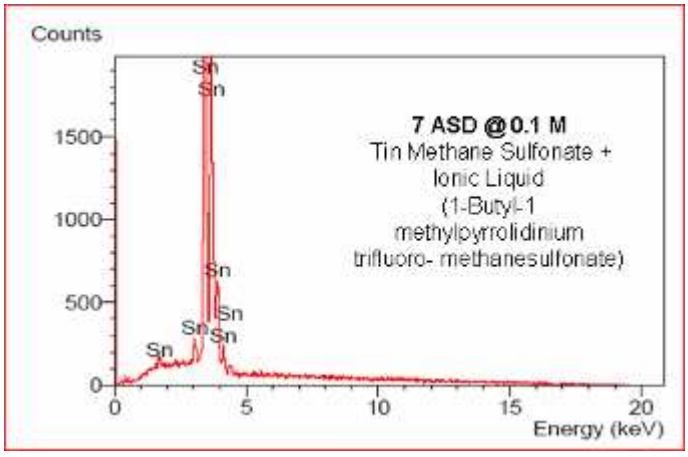

Figure 4.22: EDX for 0.1 M Sn^{2+} at BMPOTF with 7 ASD electrodeposition

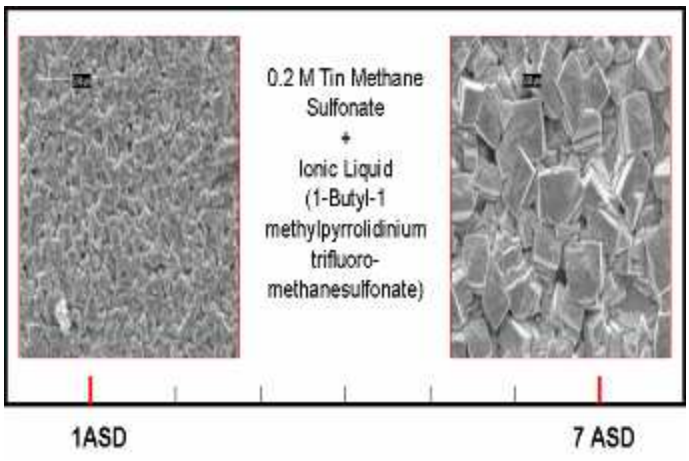

Figure 4.23: SEM for 0.2 M Sn^{2+} at BMPOTF with 1 ASD and 7 ASD electrodeposition

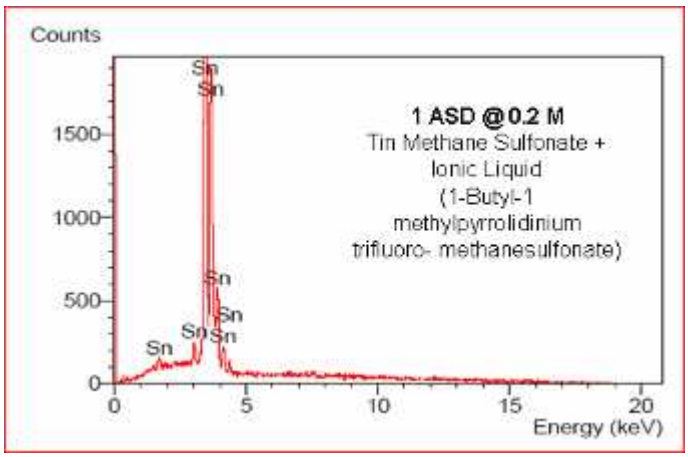

Figure 4.24: EDX for 0.2 M Sn^{2+} at BMPOTF with 1 ASD electrodeposition

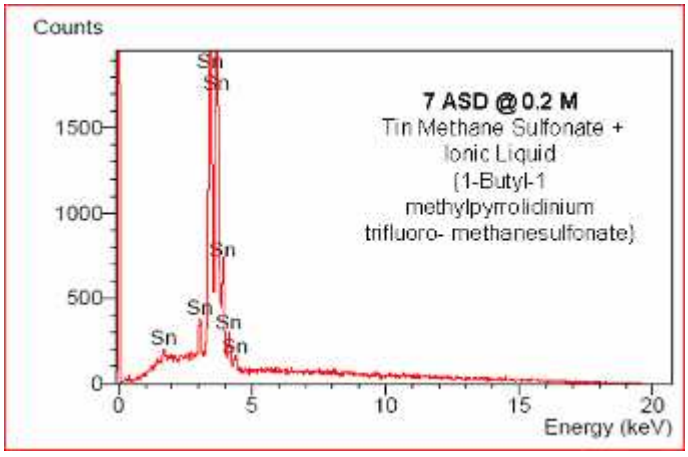

Figure 4.25: EDX for 0.2 M Sn^{2+} at BMPOTF with 7 ASD electrodeposition

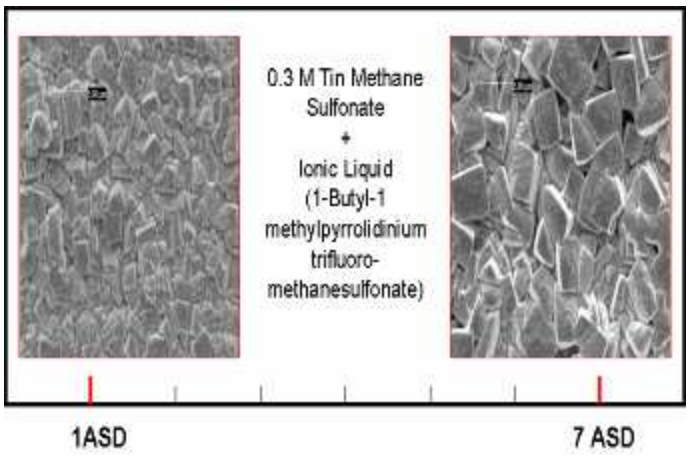

Figure 4.26: SEM for 0.3 M Sn^{2+} at BMPOTF with 1 ASD and 7 ASD electrodeposition

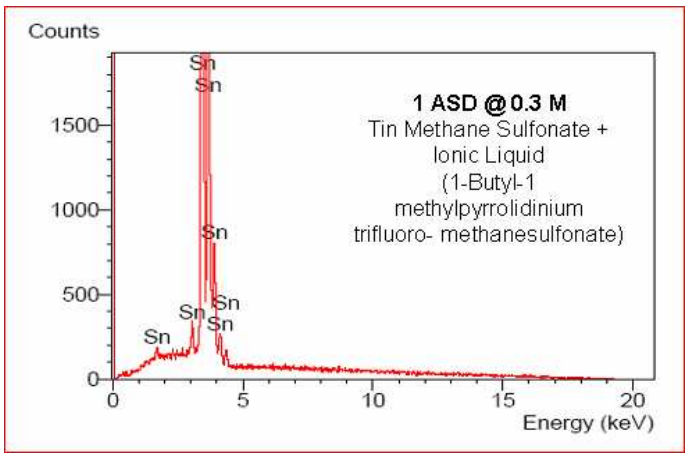

Figure 4.27: EDX for 0.3 M Sn^{2+} at BMPOTF with 1 ASD electrodeposition

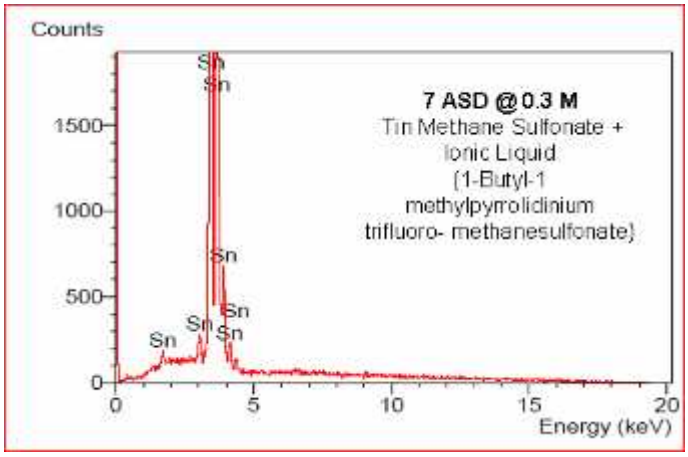

Figure 4.28: EDX for 0.3 M Sn^{2+} at BMPOTF with 7 ASD electrodeposition

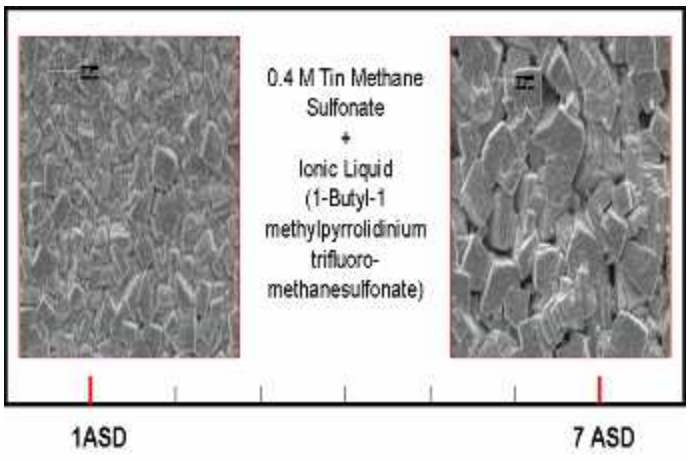

Figure 4.29: SEM for 0.4 M Sn^{2+} at BMPOTF with 1 ASD and 7 ASD electrodeposition

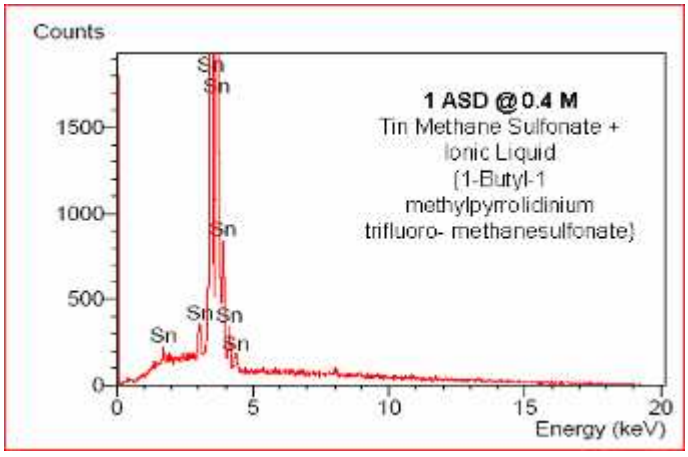

Figure 4.30: EDX for 0.4 M Sn^{2+} at BMPOTF with 1 ASD electrodeposition

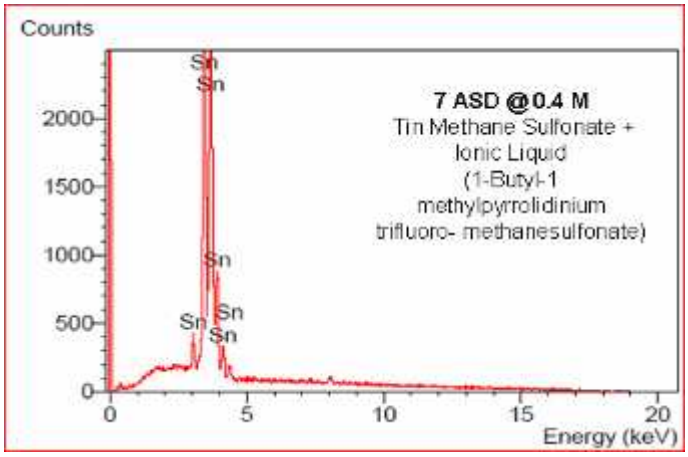

Figure 4.31: EDX for 0.4 M Sn^{2+} at BMPOTF with 7 ASD electrodeposition

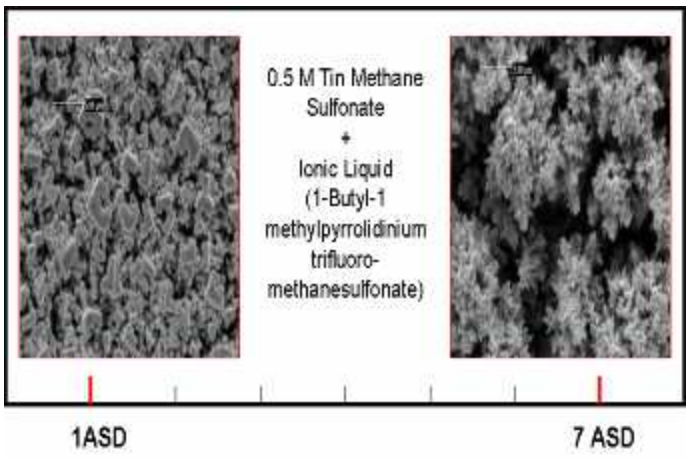

Figure 4.32: SEM for 0.5 M Sn^{2+} at BMPOTF with 1 ASD and 7 ASD electrodeposition

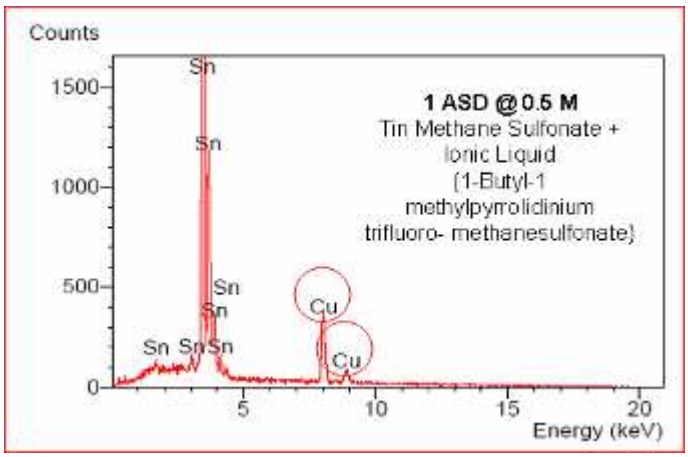

Figure 4.33: EDX for 0.5 M Sn^{2+} at BMPOTF with 1 ASD electrodeposition

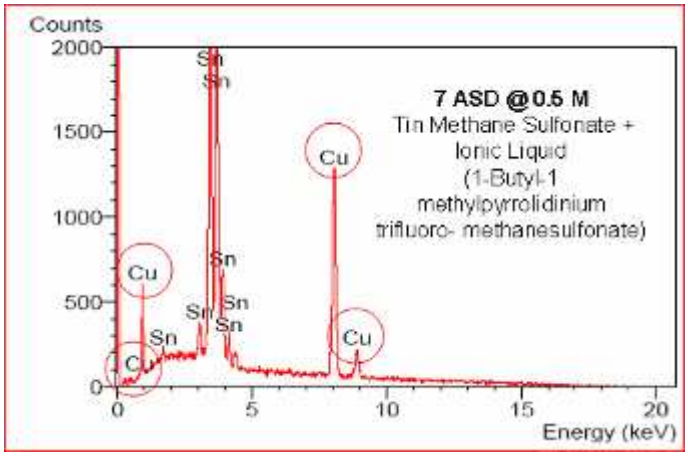

Figure 4.34: EDX for 0.5 M Sn^{2+} at BMPOTF with 7 ASD electrodeposition

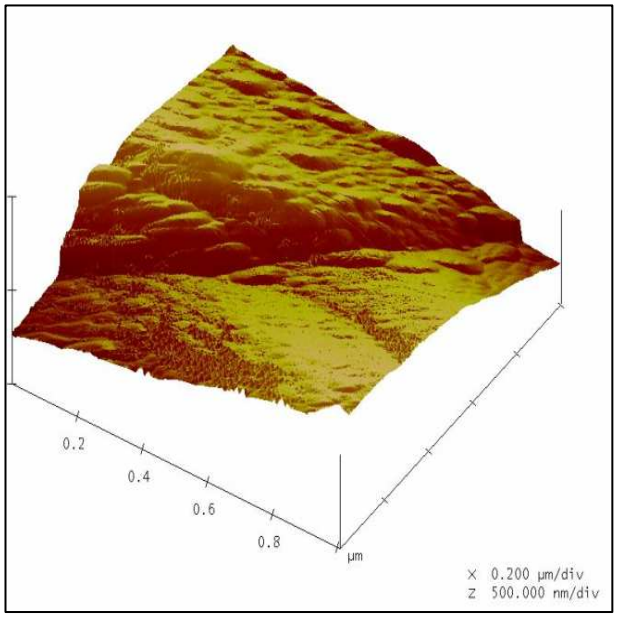

Figure 4.35: AFM for 0.1 M Sn^{2+} at BMPOTF with 7 ASD electrodeposition

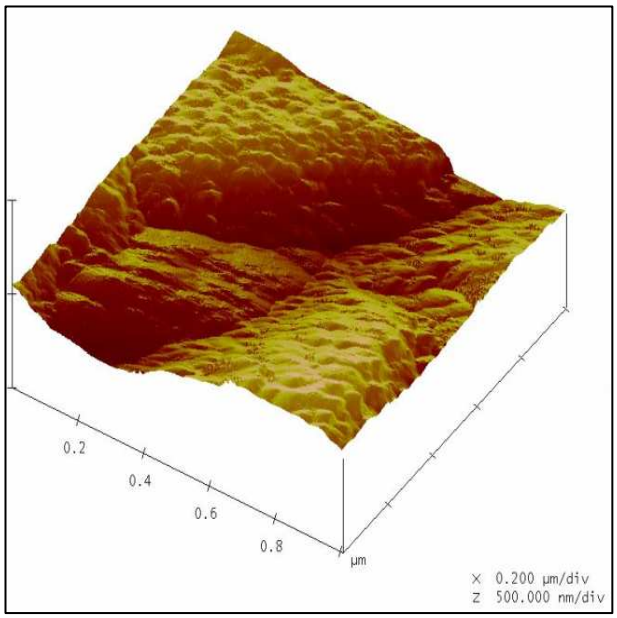

Figure 4.36: AFM for 0.2 M Sn^{2+} at BMPOTF with 7 ASD electrodeposition

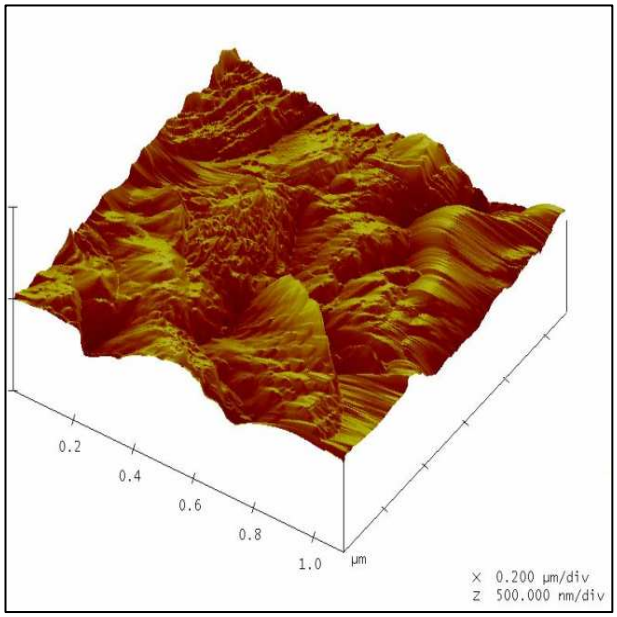

Figure 4.37: AFM for 0.3 M Sn^{2+} at BMPOTF with 7 ASD electrodeposition

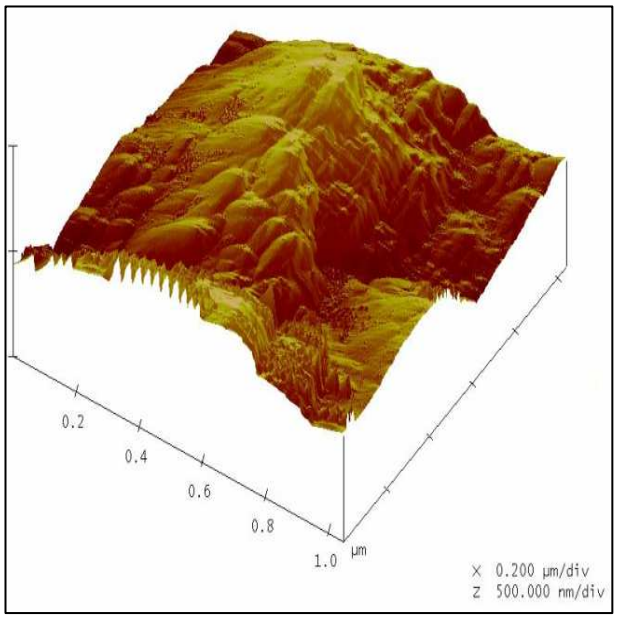

Figure 4.38: AFM for 0.4 M Sn^{2+} at BMPOTF with 7 ASD electrodeposition

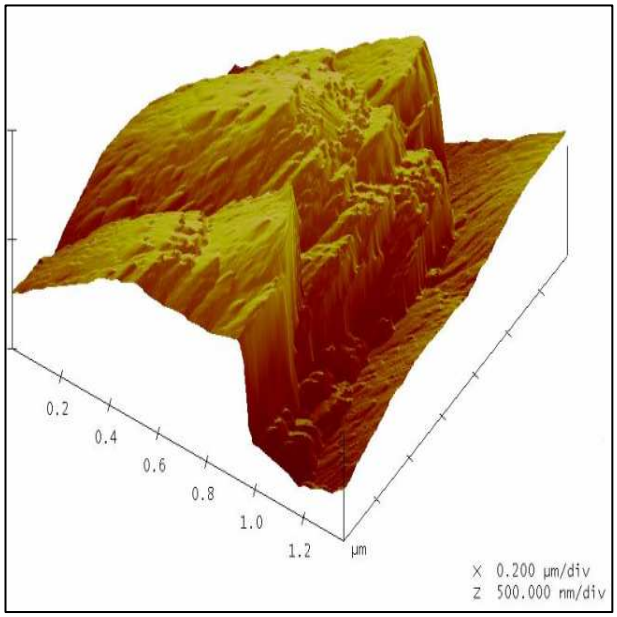

Figure 4.39: AFM for 0.5 M Sn^{2+} at BMPOTF with 7 ASD electrodeposition

4.4 FTIR analysis on electrolyte

Ionic liquid, 1-butyl-1-methyl-pyrrolidinium trifluoro-methanesulfonate, (BMPOTF) as well as the mixture of BMPOTF and Tin Methane Sulfonate, $(CH_2SO_3)_2Sn$ with various stannous ions concentration were examined using Fourier Transform Infrared (FTIR) analysis. The IR spectra of blank solution with 0 M stannous ions was presented in **Figure 4.40**, infrared spectrum with 0.1 M and 0.5 M of Stannous ions were revealed in **Figure 4.41** and **4.42** respectively.

The free O-H stretch, a sharp peak at 3600-3500 cm^{-1} are presented at all infrared spectrum, from **Figure 4.40-4.42**. Based on the FTIR result, it could be concluded that water was presented in all samples. However, the absorption of infrared radiation or the percent transmittance (%T) is getting stronger with the increasing of stannous ions. Based on the chemical technical data sheet, Tin Methane Sulfonate, $(CH_2SO_3)_2Sn$ contains 30% of water. Water content would be introduced together with tin methane sulfonate into electrolyte by means of increasing the stannous concentration.

On the other hand, the absorption of infrared radiation for sulfonate ions, with S=O stretch which occurs at 1150-1350 cm^{-1} and S-O stretch at 630-650 cm^{-1} was increased proportionally with the increasing of stannous concentration. The phenomenons are attributable to sulfonate ions and methane sulfonic acid in tin methane sulfonate. Based on the chemical technical data sheet, Tin Methane Sulfonate, $(CH_2SO_3)_2Sn$ contains 15% of Methane sulfonic acid. It means the acid concentration will increase proportionally with the tin methane sulfonate in electrolyte.

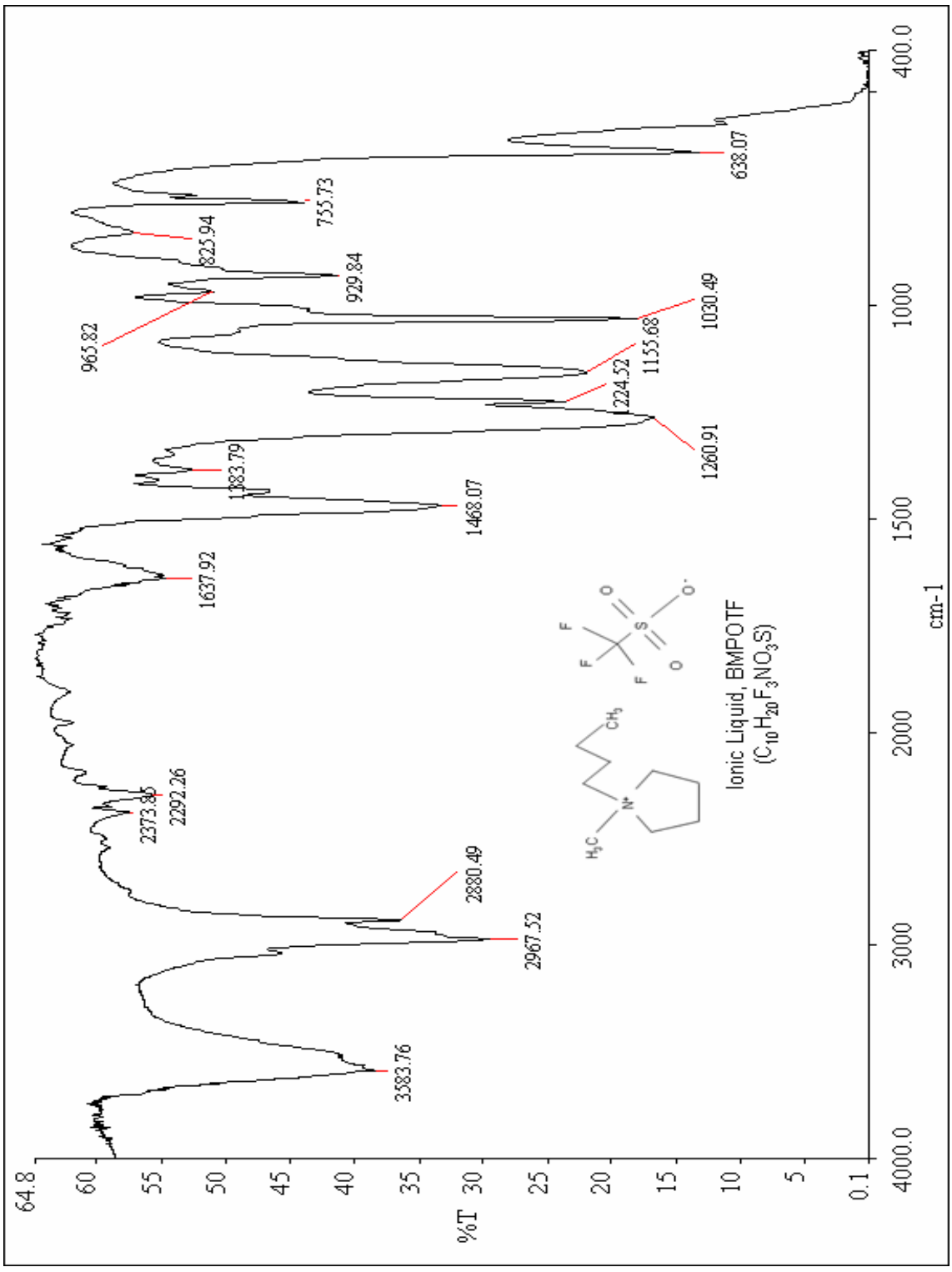

Figure 4.40: FTIR of pure Ionic Liquid – BMPOTF only

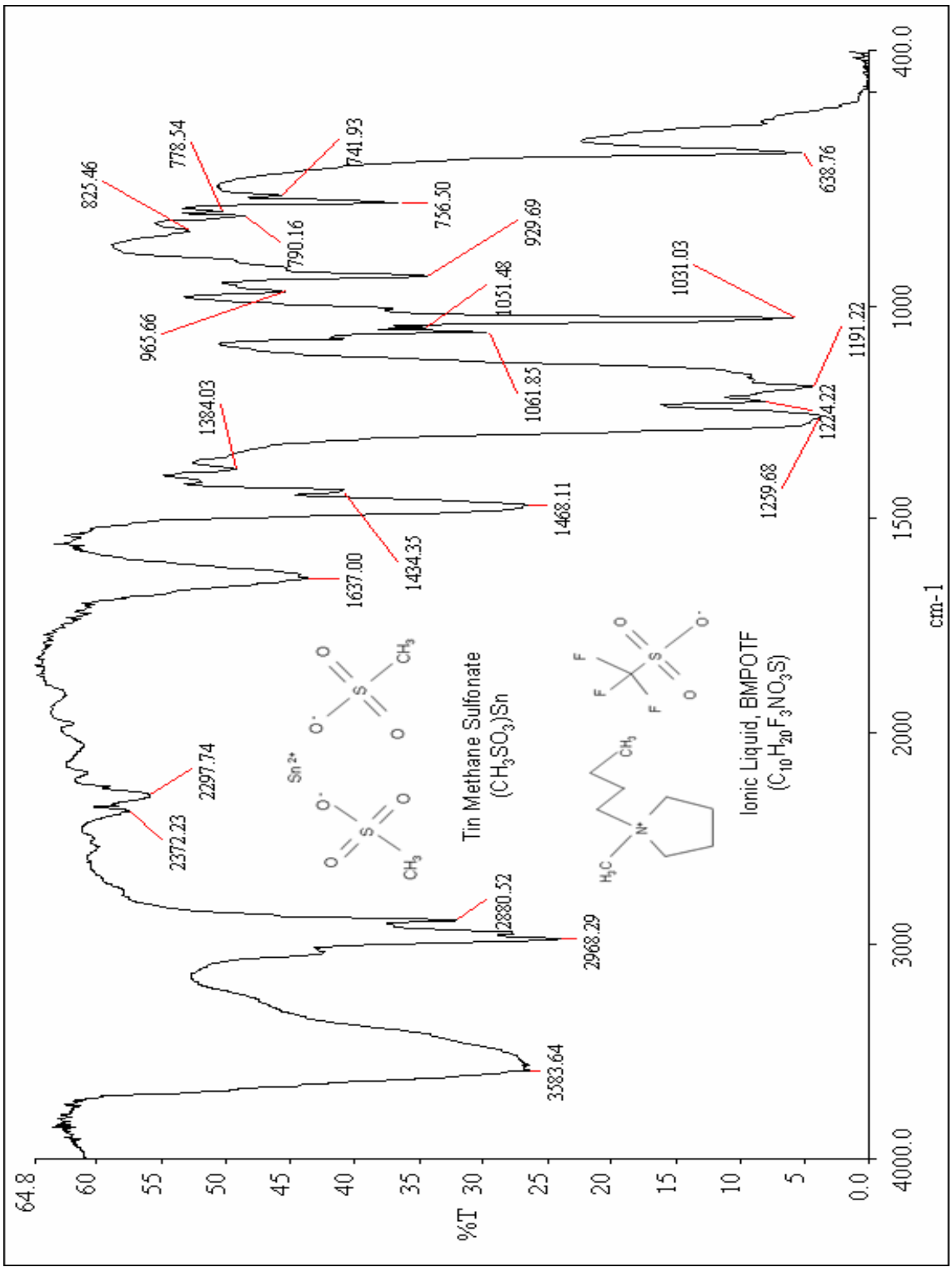

Figure 4.41: FTIR of Mixture of Ionic Liquid – BMPOTF and 0.1 M Tin Methane Sulfonate

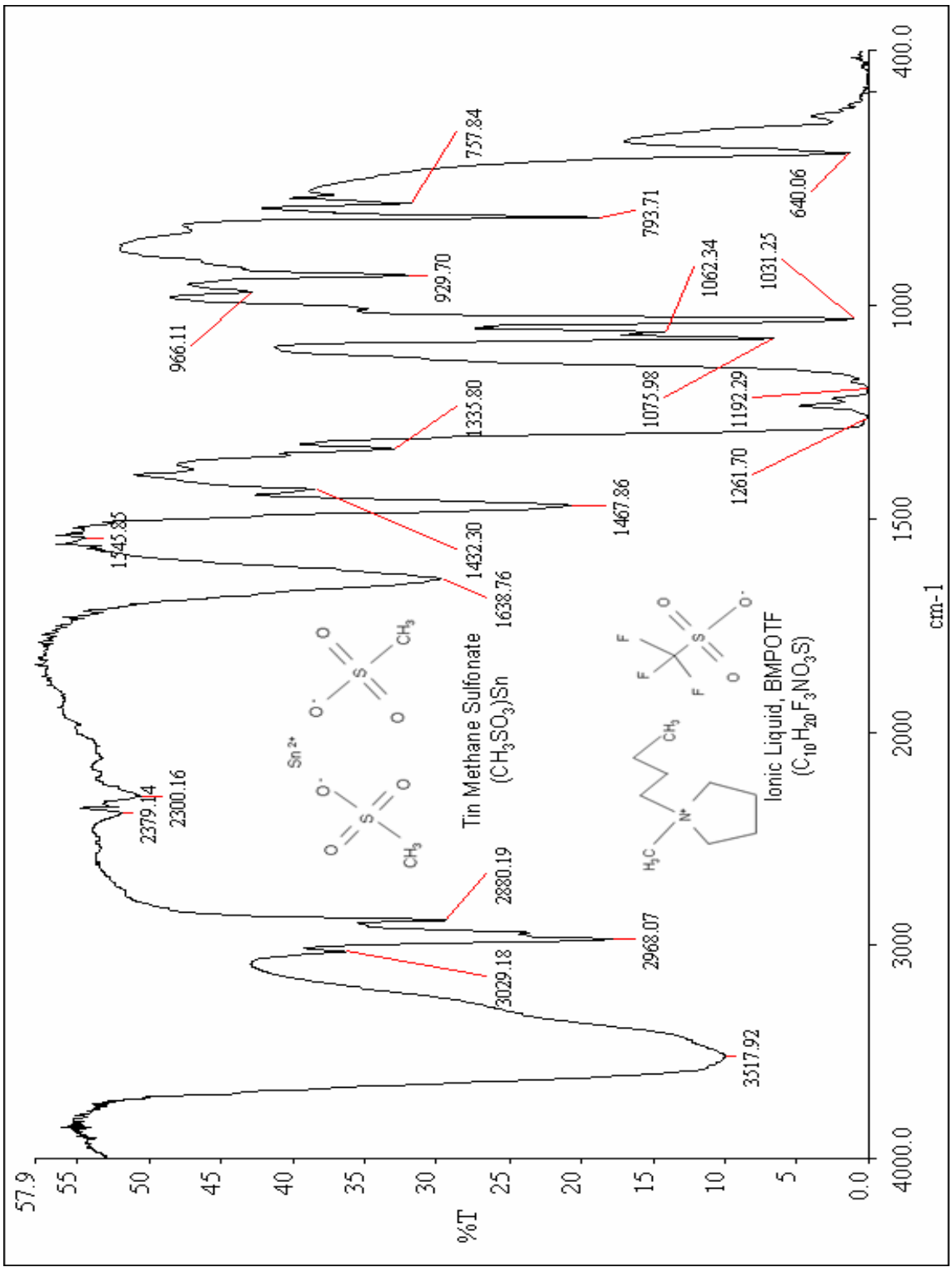

Figure 4.42: FTIR of Mixture of Ionic Liquid – BMPOTF and 0.5 M Tin Methane Sulfonate

4.5 Reliability Test

4.5.1 Results and Discussion for Wetting Balance Test

Wetting balance test had been carried out on the copper panels with dimension 20 mm X 20 mm that electrodeposited with 0.4 M Sn^{2+} in different electrolyte (**Figure 4.43 and 4.44**). Group 1 was the samples that plated in the mixture of Ionic Liquid (IL) - BMPOTF and Tin MSA . Group 2 was the samples that plated in the conventional Methane Sulfonic Acid (MSA) based tin plating electrolyte with the addition of commercial proprietary additive.

Each group of Sample had been tested with

- 245 °C with Pb-free SAC (Sn-Ag-Cu) molten solder

Sample size for each group of sample is 5 units

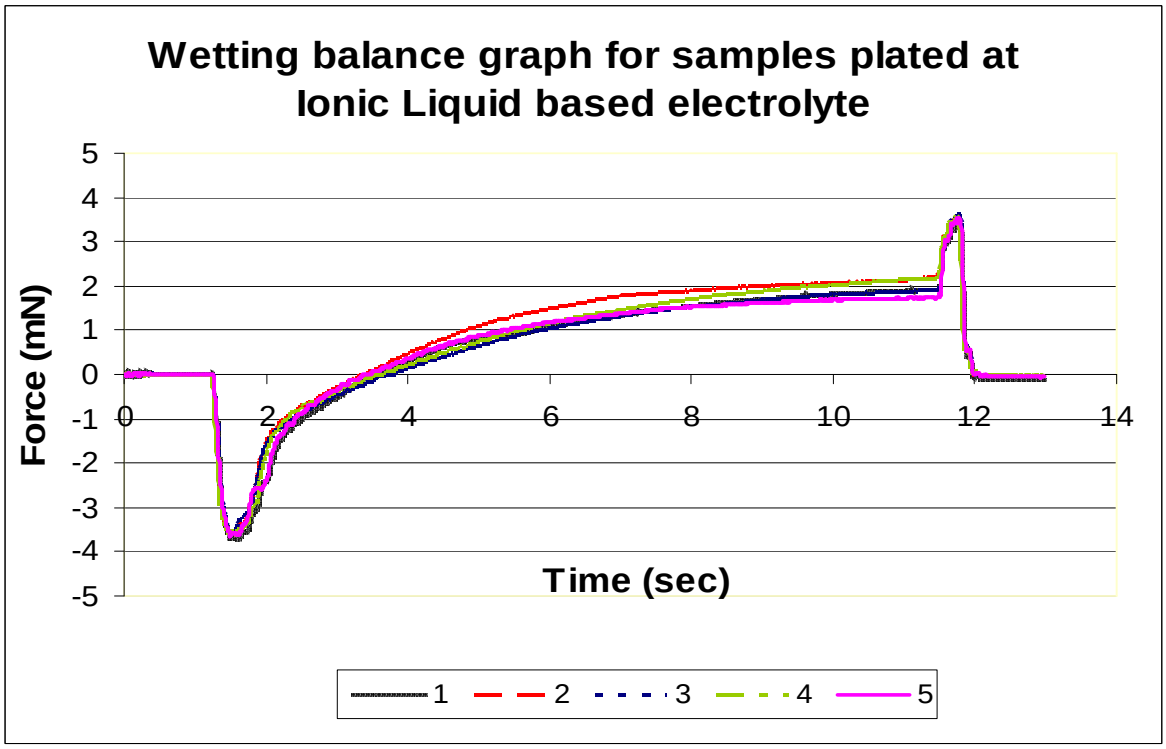

Figure 4.43: Wetting balance graph for samples plated at Ionic Liquid based electrolyte

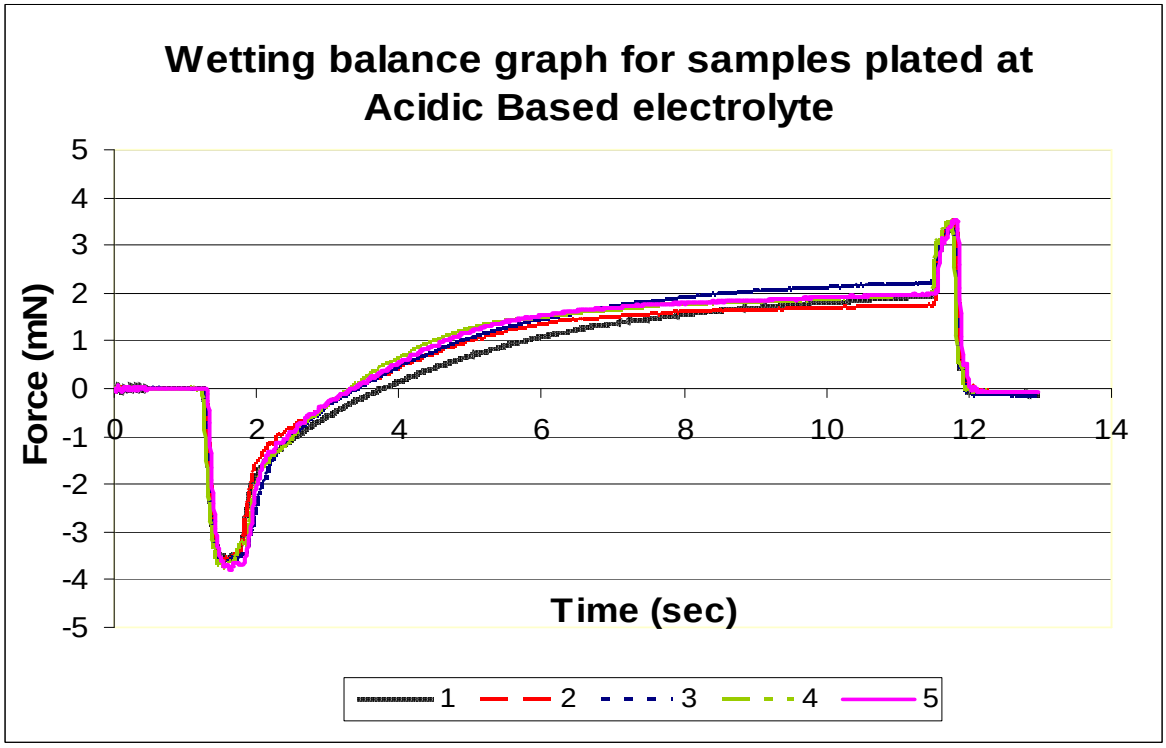

Figure 4.44: Wetting balance graph for samples plated at Acidic based electrolyte

Sample	Time-to-zero, To (Seconds)	
	IL Based (Group 1)	Acidic Based (Group 2)
1	2.331	2.152
2	2.106	2.528
3	2.460	2.184
4	2.118	2.017
5	2.203	2.085
Average	**2.244**	**2.193**

Table 4.10: Time-to-zero reading for IL based and Acidic based plated samples

In order to prove the similarity in term of solderability between IL plated and acidic (MSA) plated samples **(Table 4.10)**, hypothesis test was carried out (**Figure 4.45)**.

H_o: $u_1 = u_2$

H_1: $u_1 \neq u_2$

u_1 = wetting balance time for IL based plated samples

u_2 = wetting balance time for acidic (MSA) based plated samples

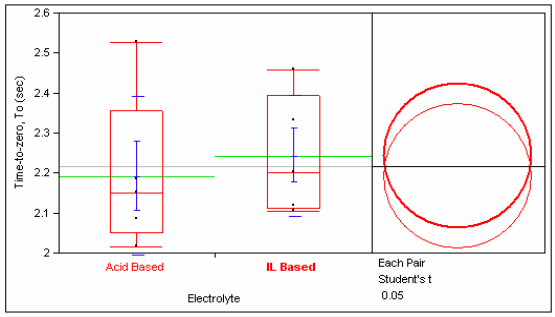

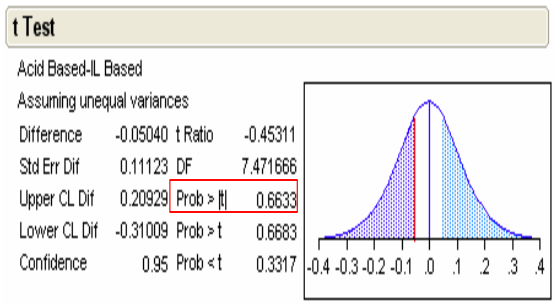

Figure 4.45: t Test diagram

From the mean comparison and t-Test diagram, p-value for t-Test is 0.6633 which is greater than 0.05; null hypothesis cannot be rejected (**Figure 4.45**). There is no significant difference in term of solderability and wetting balance time between IL plated and acidic (MSA) plated samples.